AFGL-TR-82-0079
INSTRUMENTATION PAPERS, NO. 310

Sonde Experiments for Comparative Measurements of Optical Turbulence

J.H. BROWN
R.E. GOOD
P.M. BENCH
G. FAUCHER

24 FEBRUARY 1982

AERONOMY DIVISION PROJECT 6687
AIR FORCE GEOPHYSICS LABORATORY
HANSCOM AFB, MASSACHUSETTS 01731

AIR FORCE SYSTEMS COMMAND, USAF

Unclassified

SECURITY CLASSIFICATION OF THIS PAGE (When Data Entered)

REPORT DOCUMENTATION PAGE	READ INSTRUCTIONS BEFORE COMPLETING FORM
1 REPORT NUMBER AFGL-TR-82-0070	2 GOVT ACCESSION NO AD-A118740	3 RECIPIENT'S CATALOG NUMBER
4 TITLE (and Subtitle) SONDE EXPERIMENTS FOR COMPARATIVE MEASUREMENTS OF OPTICAL TURBULENCE	5 TYPE OF REPORT & PERIOD COVERED Scientific, Interim.
	6 PERFORMING ORG. REPORT NUMBER IP, No. 319
7 AUTHOR(s) J.H. Brown G. Faucher R.E. Good P.M. Bench	8 CONTRACT OR GRANT NUMBER(s)
9 PERFORMING ORGANIZATION NAME AND ADDRESS Air Force Geophysics Laboratory (LKD) Hanscom AFB Massachusetts 01731	10 PROGRAM ELEMENT, PROJECT, TASK AREA & WORK UNIT NUMBERS 62101F 66870508
11 CONTROLLING OFFICE NAME AND ADDRESS Air Force Geophysics Laboratory (LKD) **Hanscom AFB** **Massachusetts 01731**	12 REPORT DATE 24 February 1982 13 NUMBER OF PAGES 46
14 MONITORING AGENCY NAME & ADDRESS(if different from Controlling Office)	15 SECURITY CLASS. (of this report) Unclassified 15a DECLASSIFICATION/DOWNGRADING SCHEDULE

16 DISTRIBUTION STATEMENT (of this Report)

Approved for public release; distribution unlimited.

17 DISTRIBUTION STATEMENT (of the abstract entered in Block 20, if different from Report)

18 SUPPLEMENTARY NOTES

19 KEY WORDS (Continue on reverse side if necessary and identify by block number)

Optical turbulence	Balloon
Refractive structure constant	Scintillometer
Radar turbulence	Radiosonde
Thermosonde	Turbulence
Micro-thermal probes	

20 ABSTRACT (Continue on reverse side if necessary and identify by block number)

Five different instruments were used in multiple experiments to measure atmospheric turbulence in the form of the refractive structure constant, C_n^2. These included UHF radar, optical scintillometer, modified radiosondes, AFGL thermosondes, and aircraft micro-thermal measurements. Described here are the radiosonde and thermosonde electronics and their calibrations. The data reduction scheme is described and a brief program description is given. Although the different instruments gave measurements somewhat

DD FORM 1473

Unclassified

SECURITY CLASSIFICATION OF THIS PAGE (When Data Entered)

20. Abstract (Continued)

separated in space and time, first results show good agreement between the radar, scintillometer, and thermosonde measurements.

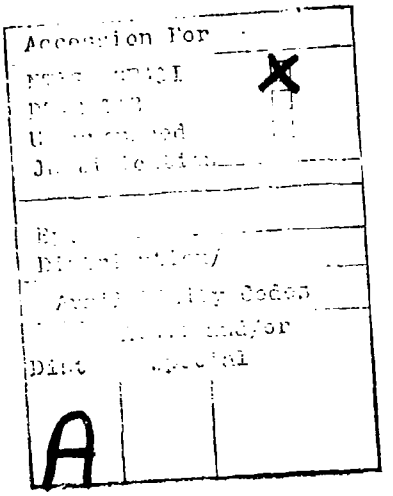

Preface

This program owes its success to the dedication of numerous individuals. These include:

Thermosonde construction and Radiosonde modification	Mr. Hans Laping, LCC Mrs. Evelyn Haynor, LCC MSGT N.K. Newman, LCC Mr. G. Murphy, Tri-Con Assoc., Inc.
Radiosonde tuning and tracking	Mr. J. Griffin, LCR Mr. K. Walker, LCR
Radar observations	Dr. Brenton Watkins, Univ. of Alaska Mr. G. Loriot, NEROC Dr. Prabhat Rostogi, NEROC
Scintillometer observations	Dr. A. Quesada, LKD
Radiosonde balloon launch	Mr. G. McPhetres, LCC MSGT J. Gordon, LCC
Tracking data reduction	Mr. Brian Sullivan, Boston College
Theoretical discussions	Dr. Edmond Dewan, LKD

We sincerely thank the many named and unnamed individuals who in large or small part contributed of themselves so willingly.

Contents

1. INTRODUCTION 7

2. RAWINSONDE 8

2.1 Rawinsonde Modifications 9
2.1.1 Met Circuit Card 9
2.1.2 Transponder Receiver 9
2.1.3 Transmitter 10
2.2 Resistance Calculation 10
2.2.1 Temperature Calibration 11
2.2.2 Humidity Calibration 11
2.2.3 Pressure Calibration 12

3. THERMOSONDE 14

3.1 Thermosonde Description 14
3.2 Sensor Heating Effects 17
3.3 Sensor Frequency Response 20
3.4 Thermosonde Calibration 21
3.5 Thermosonde Environment 21

4. DATA REDUCTION 23

4.1 Time Period Records 24
4.2 Reference Frequency ID 24
4.3 Segment Window ID 24
4.4 Tracker Data 25

5. PROGRAM DESCRIPTION 26

6. RESULTS 31

REFERENCES 45

Illustrations

1.	**Sample Output of Reduced Radiosonde/Thermosonde Data**	13
2.	Photograph of Thermosonde and Micro-thermal Probe	16
3.	Schematic of Thermosonde Sensor Convective Heat Transfer Test Circuit	18
4.	Heat Transfer Coefficient Curve of Thermosonde Sensor as a Function of Altitude	19
5.	Calibration Curve of Thermosonde Sensor ΔR as a Function of Radiosonde Frequency	22
6.	Calibration Curve of Thermosonde $(\Delta T)_{RMS}$ as a Function of Radiosonde Frequency	22
7.	Sample Output of Reduced Tracker Data	27
8.	Typical Temperature Profile Plot	31
9.	Typical Relative Humidity Profile Plot	32
10.	Typical Balloon Velocity Analysis – East Profile Plot	33
11.	**Typical Balloon Velocity Analysis – North Profile Plot**	33
12.	**Typical Horizontal Vector Shear Analysis Profile Plot**	34
13.	Expanded View of Horizontal Vector Shear	34
14.	Power Spectral Density Analysis of Horizontal Vector Shear	35
15.	Raw Thermosonde C_N^2 Analysis – Profile Plot	37
16.	Expanded View of Raw Thermosonde C_N^2 Profile Plot	38
17.	Smoothed Thermosonde C_N^2 Profile Plot	39
18.	Cumulative Probability Distribution Curve of Log C_T^2	40
19.	Comparison of Radar C_N^2 and Scintillometer C_N^2 Profiles	41
20.	Scintillometer Weighting Functions	42
21.	Comparison of Thermosonde C_N^2 and Scintillometer C_N^2 Profiles	43
22.	Comparison of Thermosonde C_N^2 and Radar C_N^2 Profiles	44

Tables

1.	Optical C_N^2 (Turbulence) Measurement Program	28

Sonde Experiments for Comparative Measurements of Optical Turbulance

1. INTRODUCTION

Atmospheric properties of temperature, pressure, humidity, and wind speed, as measured by meteorological radiosondes, offer a means of estimating the fluctuations in the atmospheric optical index of refraction. Fluctuations of the index of refraction, characterized as C_N^2, are important to numerous DOD optical systems being both planned and developed. Direct measurements of C_N^2 are possible with optical systems such as those used to evaluate sites for astronomical telescopes. These measurements have been limited to a few locations, and this technique is not suitable for assembling a world wide data base of C_N^2. Given that C_N^2 determined from meteorological data can be an accurate measure of optical turbulence, the best promise for economically assembling a large data base is through the use of the archived meteorological sounding data obtained from sondes.

The present rawinsonde measurements are usually achieved with altitude resolution of 300 m or larger. This scale is generally accepted as being larger than the vertical scales of turbulence that produce the C_N^2. Thus, in order to develop an analytical model predicting C_N^2 from the standard rawinsonde, it is necessary to have a statistical base relating the actual turbulence scales to the rawinsonde observed scales. New sondes (artsondes) have been developed by VIZ Corporation for the National Weather Service to measure the meteorological

(Received for publication 19 February 1982)

variables at smaller altitude resolution. These sondes were modified at AFGL to provide data for a C_N^2 intercomparison test. The program objective is to compare C_N^2 as determined from standard rawinsondes, the AFGL modified artsondes, AFGL built thermosondes, stellar scintillometers, aircraft-mounted commercial thermosondes, and UHF radar.

The detailed description of the AFGL artsonde and thermosonde is presented in this report. Also presented is the calibration procedure and the computer analysis used to derive the meteorological values from the recorded telemetry signal. The sonde tracking and ranging system is described along with the data processing procedures used to smooth the data and determine the winds as a function of altitude. A brief description of experimental results is shown as comparisons of C_N^2 measurements obtained with radar, optical scintillometer, and thermosonde.

2. RAWINSONDE

The rawinsonde used in these experiments consists of meteorological measuring elements coupled to a radio transmitter and assembled into a small lightweight plastic case. The device is carried aloft by a 1200-gm balloon filled with helium gas. Included in the train is a small parachute to slow the descent of the device after the balloon bursts. An automatic launching reel is attached to the train, which lowers the radiosonde until the train is fully extended to about 20 m. As the balloon ascends at about 5 m/sec, measurements of pressure, temperature, and relative humidity are transmitted to a ground station where the data are recorded. As the balloon rises, it is followed electronically by radio direction-finding equipment that tracks the transmitted signal. Measurements of the balloon position relative to the ground station are recorded in terms of azimuth, elevation, and slant range. These measurements are converted to X, Y, and Z distances. The data are filtered as described in Section 4.4 to remove extraneous signals and then time differenced to obtain wind velocity profiles.

Fifty (50) state-of-the-art radiosondes were purchased from VIZ Corporation, Philadelphia, Pa. These are called by them the "Artsonde-Phase II," and they carry VIZ part number, 1499-311. This is a 1680-MHz amplitude modulated sonde with a 403-MHz receiver used for transponder ranging. The transmission of meteorological (MET) data serially switches by solid-state circuitry from pressure to temperature, to relative humidity, to reference, and back to pressure with a segment dwell time of 250 msec. Premium sensor elements are used for the aneroid baroswitch, thermistor, and hygristor. Depending upon the sensor input resistance, a frequency of 30 to 1000 Hz is produced that modulates the 1680 MHz transmitter. The reference frequency is set close to 1000 Hz. It provides the

identification of segment position, and it allows for data correction of temperature induced frequency drifts.

2.1 Rawinsonde Modifications

After delivery of the radiosondes, several in-house modifications were required. Because greater temporal and spatial data resolution were desired than were available from a standard radiosonde and its associated GMD tracker, special payload and ground equipment changes were implemented. Additionally, a separate instrument to measure small temperature fluctuations (thermosonde) was attached physically and electrically to the radiosonde. The modification included changes in the radiosonde transmitter, receiver, solid-state switching, and MET oscillator circuit boards.

2.1.1 MET CIRCUIT CARD

In order to transmit the additional thermosonde data, the number of commutation data segments was increased from the standard four to eight. To accomplish this, a second quad-bilateral switch (p/n 4066) was added to the MET circuit board. This was facilitated by the existing 4017 IC clock, which allows serial switching of up to ten segments. Two of the additional segments were used for thermosonde information and two were used as auxilliary segments. The auxillary segments allowed super-commutation of the MET data or the reporting of electronics temperature.

To accomplish calibration and ground-base checks the eight lock-up and one common test points were brought to an eight-position rotary switch. During calibration the normally free-running segment switch was stopped on a segment corresponding to the position of the switch. The frequency of each segment was examined, in turn, by rotating the switch from one position to the next. The measured frequency was then recorded along with the measured temperature, humidity, pressure commutator position, and thermosonde test value. The baroswitch that forms one part of the MET board transmits one of four unique frequencies depending upon the position of the baroswitch armature. The original separation of frequencies was only 10 or 20 Hz. In order to provide a separation of 100 Hz between each frequency, three new resistors replaced existing ones with appropriate values. This reduced confusion over contact identification.

2.1.2 TRANSPONDER RECEIVER

The balloon borne 403-MHz transponder receiver is used to derive the slant range in the following manner: Ground-base equipment generates a PCM code that is synchronized with the start pulse of a time interval counter. This code modulates the 403-MHz uplink transmitter. The receiver transponder uses this code to

modulate a 70-kHz subcarrier oscillator. This subcarrier is mixed with the MET data and used to modulate the balloon-borne transmitter. Ground-base equipment retrieves and decodes the PCM code, which then sends a stop pulse to the interval counter. Since slant range is calibrated vs interval, a direct digital coded range output is produced.

2.1.3 TRANSMITTER

Normally the transmitter is 100 percent amplitude modulated by the MET data pulses. When the MET data pulse is high, the transmitter is shut down. This results in an AM pulse repetition frequency that is measured by ground receiving equipment to determine the sensor input resistance.

The on-board 403-MHz receiver frequency modulates the transmitter. Since this information is lost when the MET signal is high (because the transmitter is shut down), difficulty in holding synchronization to the ranging signal develops. Consequently the evaluation of slant range data contains associated errors. To eliminate this problem, the ac-coupling AM input to the transmitter was removed. Instead, the MET data was ac-coupled to the transmitter in the same manner and to the same junction point as the ranging signal. This results in MET data frequency modulation of 30 to 1000 Hz and ranging modulation of 70 kHz.

2.2 Resistance Calculation

This section presents the MET data transfer equations as given by VIZ Corporation (document nos. VIZ 800721 and 761101B). The form of these expressions as well as the constants depend on the sensor type and manufacturing lot number. The input resistance to the radiosonde corresponding to the measured MET frequency is:

$$R_{input} = R_{int} (f_{ref}/f_{meas} - 1) ,$$

where f_{ref} is the average measured reference frequency and f_{meas} is the average measured segment frequency when the baroswitch in on a space (that is, between two discrete contact points).

The thermistor or pressure resistance is the input resistance when on a temperature or pressure segment.

The input resistance when on a humidity segment is the equivalent parallel resistance of a 1-M resistor and the hygristor resistance; thus,

$$R_{RH} = \frac{R_{input} \times 10^6}{1 \times 10^6 - R_{input}} .$$

2.2.1 TEMPERATURE CALIBRATION

Temperature is calculated from the thermistor resistance R_T as follows:

$$t_{°c} = \frac{1}{\sum_{k=o}^{3} A_k \{\ln (R_T/R_{30})\}^k} - 273.15 ,$$

where R_{30} is the acculok lock-in resistance at 30°C. The coefficients for premium temperature element lot P6970 as provided by VIZ are:

A_o = 3.2987 E-03

A_1 = 4.7610 E-04

A_2 = 2.8417 E-06

A_3 = 1.5691 E-06 .

2.2.2 HUMIDITY CALIBRATION

Relative humidity is calculated from the hygristor resistance R_{RH} as follows:

$$RH = A - \frac{69.}{\sum_{k=0}^{4} D_k [f(R_{RH})]^k} ,$$

where

$f(R_{RH}) = f(t) \ln (R_{RH}/R_{33})$,

R_{33} is the acculok lock-in resistance at 33 percent RH and 25°C,

and

$$f(t) = \sum_{k=o}^{3} C_k (t)^k \qquad (t = {}^{o}\text{Celsius}) .$$

The coefficients for premium humidity element lot 2265 as provided by VIZ are:

for $R_{RH}/R_{33} \geq 1$:	for $R_{RH}/R_{33} < 1$:
C_o = 7.885 E-01	C_o = 9.243 E-01
C_1 = 9.286 E-03	C_1 = 3.059 E-03
C_2 = -2.462 E-05	C_2 = -1.188 E-06
C_3 = -3.368 E-07.	C_3 = 0.

for $f(R_{RH}) \geq -0.2$:	for $f(R_{RH}) < -0.2$:
D_o = 1.	D_o = -2.0909 E00
D_1 = 7.1454 E-01	D_1 = 9.2406 E00
D_2 = -7.9163 E-02	D_2 = 2.1693 E01
D_3 = 3.2555 E-02	D_3 = 2.2214 E01
D_4 = 3.9255 E-03	D_4 = -6.1926 E00
A = 102.	A = 0.

2.2.3 PRESSURE CALIBRATION

Each radiosonde is provided with pressure calibration values for the leading edge of 160 contact positions of the baroswitch by VIZ Corporation. Four discrete frequencies can be transmitted by the baroswitch, depending upon at which of the four classifications of contacts the baroswitch is located. The four frequencies were adjusted to provide approximately 500-, 600-, 700-, and 800-Hz signals. Approximately 500 Hz is transmitted when the baroswitch is located between any two discrete contact points. Approximately 600 Hz is transmitted for the following contact numbers: 30, 45, 60, 75, 90, 105, 120, 135, 140, 145, 150, 155, and 160. These start at contact number 30 and increase by 15 for contact numbers less than 135 and increase by five for contact numbers greater than 135. Approximately 700 Hz is transmitted for the following contact numbers: 5, 10, 15, 20, 25, 35, 40, 50, 55, 65, 70, 80, 85, 95, 100, 110, 115, 125, 130, 136, 137, 138, 139, 141, 142, 143, 144, 146, 147, 148, 149, 151, 152, 153, 154, 156, 157, 158, and 159. These start at contact number 5 and increase by five for contact numbers less than 135 and increase by one for contact numbers greater than 135. Approximately 800 Hz is transmitted for all other contacts. Before each launch the baroswitch is manually set to the contact position corresponding to the ambient station pressure. During analysis the computer identifies groups and subgroups of contacts and defines a particular contact within a larger group. Thus, if transmission is lost for a short time, the computer redefines the location of the baroswitch and estimates the present contact number. Pressure is defined at the leading edge of each contact and is logarithmically interpolated between contacts based on altitude.

Sample results of the pressure, temperature, humidity, and C_N^2 calculations are presented in Figure 1. The first column is the record number. "Time" is defined as seconds after launch. "CTEMP" is the corrected temperature based on inferred time lags. No correction is made to humidity below -40°C. Pressure contacts are split into classes 0 to 3. Column 11 shows that a contact number is defined at the first encounter of a new contact. Columns 14 and 16 show that

RAWINSONDE FREQ QX0020 LAUNCH 12812.00 JUL 212812.00 LOCAL REF FREQ 1008.0 12 /81

TIME SAMPLE C 00 99999.00

RO 28.60 R30 14161. R33 12019. SURFACE TEMP 15.5 19.8 PRES 1012.0 RH 63.5 ALT .1234KM

	(Sec) TIME	(Hz) REF	(°C) TEMP	(°C) DTEMP	(%) RH	(%) DRH	(km) ALT	(km) DALT	(Hz)		#	(mb) PRES	°Crms LOW	$(m^{2.3})$ CN	°Crms MID	$(m^{2.3})$ CN	
1508	3055.77	985.7	-58.7	-58.7	20.3	999.0	15.32	15.31	508.0	0	-999	124.3	.0028	3.540E-19	.0053	1.301E-18	
1509	3057.80	986.8	-58.8	-58.6	20.4	999.0	15.33	15.32	508.1	0	-999	124.2	******-9	9.990E+02	.0049	1.107E-18	
1510	3059.82	987.4	-58.6	-58.4	20.5	999.0	15.34	15.33	508.0	0	-999	124.0	.0162	1.180E-17	.0242	2.653E-17	
1511	3061.87	986.0	-58.6	-58.5	20.4	999.0	15.34	15.34	507.5	0	-999	123.9	.0079	2.788E-18	.0154	1.072E-17	
1512	3063.91	985.4	-58.6	-58.6	20.4	999.0	15.35	15.35	507.4	0	-999	123.7	******-9	9.990E+02	.0071	2.240E-18	
1513	3065.93	986.7	-58.5	-58.5	20.4	999.0	15.36	15.35	507.3	0	-999	123.6	.0083	3.110E-18	.0046	3.288E-18	
1514	3067.96	987.7	-58.6	-58.6	20.4	999.0	15.37	15.36	604.2	3	120	123.4	.0134	8.025E-18	.0179	1.433E-17	
1516	3072.03	988.2	-58.6	-58.7	20.5	999.0	15.39	15.38	603.9	3	-999	123.0	.0167	1.252E-17	.0252	2.835E-17	
1517	3074.04	985.9	-58.6	-58.5	20.3	999.0	15.40	15.39	604.2	3	-999	122.8	.0101	4.554E-18	.0148	1.737E-17	
1518	3076.09	987.5	-58.6	-58.7	20.3	999.0	15.41	15.40	604.0	3	-999	122.6	.0029	3.845E-19	.0042	3.007E-18	
1519	3078.11	985.3	-58.6	-58.5	20.2	999.0	15.42	15.41	-999.0	-99	-999	122.4	.0026	3.060E-19	.0065	1.845E-18	
1520	3080.15	987.0	-58.7	-58.9	20.4	999.0	15.43	15.42	507.8	0	-999	122.2	******-9	9.990E+02	.0046	9.499E-19	
1521	3082.18	986.1	-58.8	-59.0	20.5	999.0	15.44	15.43	508.1	0	-999	122.1	******-9	9.990E+02	.0028	3.425E-19	
1522	3084.27	986.8	-58.7	-58.7	20.4	999.0	15.45	15.44	508.3	0	-999	121.9	******-9	9.990E+02	.0035	5.470E-19	
1523	3086.24	986.3	-58.6	-57.9	20.3	999.0	15.46	15.45	506.8	0	-999	121.7	.0073	2.298E-18	.0127	6.904E-18	
1524	3088.27	987.7	-58.6	-58.7	20.4	999.0	15.47	15.46	507.9	0	-999	121.5	.0071	2.224E-18	.0119	6.162E-18	
1525	3090.31	986.9	-58.6	-58.6	20.4	999.0	15.48	15.47	507.7	0	-999	121.3	******-9	9.990E+02	.0055	1.302E-18	
1526	3092.33	989.0	-58.6	-58.4	20.6	999.0	15.49	15.48	507.8	0	-999	121.1	.0067	1.955E-18	.0052	1.165E-18	
1527	3094.37	986.6	-58.6	-58.6	20.4	999.0	15.50	15.49	507.2	0	-999	120.9	.0133	7.624E-18	.0155	1.028E-17	
1528	3096.40	986.6	-58.6	-58.6	20.4	999.0	15.51	15.50	507.4	0	-999	120.7	.0056	1.368E-18	.0111	5.251E-18	
1529	3098.43	986.6	-58.6	-58.6	20.4	999.0	15.52	15.51	507.1	0	-999	120.5	******-9	9.990E+02	.0056	1.340E-18	
1530	3100.47	988.2	-58.6	-58.6	20.4	999.0	15.53	15.52	507.1	0	-999	120.4	.0042	7.484E-19	.0039	6.644E-19	
1531	3102.50	987.9	-58.6	-58.8	20.5	999.0	15.54	15.53	507.2	0	-999	120.2	.0047	9.262E-19	.0091	3.501E-18	
1532	3104.53	985.1	-58.7	-59.2	20.3	999.0	15.55	15.54	507.5	0	-999	120.0	.0078	2.623E-18	.0111	5.251E-18	
1533	3106.56	987.0	-58.8	-58.8	20.4	999.0	15.56	15.55	507.6	0	-999	119.8	.0211	1.893E-17	.0128	6.979E-18	
1534	3108.60	985.0	-58.7	-58.7	20.2	999.0	15.57	15.56	800.3	1	121	119.6	.0299	3.774E-17	.0351	5.201E-17	
1535	3110.62	986.6	-58.7	-58.7	20.5	999.0	15.57	15.57	800.7	1	-999	119.5	.0341	4.899E-17	.0476	9.560E-17	
1536	3112.68	985.6	-58.7	-58.6	20.5	999.0	15.58	15.58	800.4	1	-999	119.3	.0165	1.141E-17	.0234	2.921E-17	
1537	3114.68	986.0	-58.6	-58.5	20.5	999.0	15.59	15.58	800.5	1	-999	119.2	.0305	3.880E-17	.0224	2.099E-17	
1538	3116.72	986.6	-58.6	-58.7	20.4	999.0	15.60	15.59	801.3	1	-999	119.0	.0842	2.957E-16	.0448	1.037E-16	****
1539	3118.79	987.0	-58.6	-58.6	20.4	999.0	15.60	15.60	800.4	1	-999	118.9	.0280	3.[illegible]E-17	.0505	1.060E-16	
1540	3120.77	985.7	-58.5	-58.3	20.3	999.0	15.61	15.61	800.6	1	-999	118.7	.0123	6.198E-18	.0259	2.765E-17	
1541	3122.81	986.8	-58.5	-58.4	20.4	999.0	15.62	15.61	800.6	1	-999	118.6	.0047	9.139E-19	.0110	4.970E-18	
1542	3124.85	985.7	-58.5	-58.6	20.2	999.0	15.63	15.62	507.5	0	-999	118.4	.0043	7.666E-19	.0109	4.872E-18	
1543	3126.87	985.0	-58.6	-58.8	20.3	999.0	15.64	15.63	508.0	0	-999	118.3	******-9	9.990E+02	.0041	6.907E-19	
1544	3128.90	985.4	-58.5	-58.4	20.4	999.0	15.64	15.64	507.5	0	-999	118.1	******-9	9.990E+02	.0033	4.548E-19	
1545	3130.95	986.6	-58.5	-58.3	20.4	999.0	15.65	15.65	507.5	0	-999	118.0	******-9	9.990E+02	.0053	1.130E-18	
1546	3132.97	986.5	-58.5	-58.5	20.5	999.0	15.66	15.65	507.7	0	-999	117.8	******-9	9.990E+02	.0020	1.634E-19	
1547	3134.99	987.4	-58.4	-58.3	20.5	999.0	15.67	15.66	507.6	0	-999	117.7	******-9	9.990E+02	******-9	9.990E+02	
1548	3137.06	987.1	-58.4	-58.2	20.4	999.0	15.68	15.67	507.2	0	-999	117.5	.0035	4.361E-19	.0052	1.545E-18	
1549	3139.07	985.8	-58.4	-58.5	20.3	999.0	15.68	15.68	507.4	0	-999	117.4	.0025	2.550E-19	.0074	2.210E-18	
1550	3141.09	984.5	-58.5	-58.5	20.2	999.0	15.69	15.69	507.6	0	-999	117.2	.0028	3.158E-19	.0087	3.026E-18	
1551	3143.13	987.5	-58.4	-58.2	20.5	999.0	15.70	15.69	507.4	0	-999	117.1	.0025	2.522E-19	.0031	3.962E-19	
1552	3145.16	986.1	-58.4	-58.5	20.4	999.0	15.71	15.70	507.6	0	-999	117.0	******-9	9.990E+02	.0027	2.908E-19	
1553	3147.19	984.6	-58.4	-58.4	20.3	999.0	15.71	15.71	507.4	0	-999	116.8	******-9	9.990E+02	.0048	9.390E-19	
1554	3149.22	987.4	-58.4	-58.3	20.4	999.0	15.72	15.72	507.8	0	-999	116.7	******-9	9.990E+02	.0027	2.952E-19	
1555	3151.25	987.1	-58.4	-58.4	20.5	999.0	15.73	15.72	508.0	0	-999	116.5	.0076	1.295E-18	.0157	1.106E-17	
1556	3153.30	984.1	-58.5	-58.6	20.3	999.0	15.74	15.73	507.9	0	-999	116.4	.0024	2.350E-19	.0072	2.078E-18	
1557	3155.32	986.1	-58.3	-58.2	20.4	999.0	15.75	15.74	507.2	0	-999	116.2	******-9	9.990E+02	.0030	3.571E-19	
1558	3157.35	988.1	-58.3	-58.3	20.5	999.0	15.75	15.75	507.3	0	-999	116.1	******-9	9.990E+02	******-9	9.990E+02	

Figure 1. Sample Output of Reduced Radiosonde/Thermosonde Data. Processed results

$(\Delta T)_{rms}$ is undefined for values less than 0.002^{o}. The "****" in the last column flag values of $(\Delta T)_{rms}$ low gain that are greater than 0.035^{o}. The corresponding high gain value is not valid for this condition.

3. THERMOSONDE

The thermosonde is a small, lightweight, temperature-sensing electronic unit that attaches to the radiosonde. It measures the difference in temperature of the ambient atmosphere between two probes mounted horizontally 1 m apart. As the balloon ascends or descends, the temperature differences are processed and routed to the radiosonde MET segments. The received data is used to calculate the atmospheric temperature structure parameter C_T^2. These data, together with pressure and temperature, are used to calculate the refractive index structure parameter C_N^2. Fundamentally, C_N^2 is defined as:[1]

$$C_N^2 = \overline{[n(\vec{r}_1) - n(\vec{r}_2)]^2}/r^{2/3} ,$$

for $n(r_i)$ the index of refraction at point r_i and $r = |\vec{r}_1 - \vec{r}_2|$. This parameter is the key unknown in estimating the performance of laser systems through the clear atmosphere. Among those explicit or indirect dependencies on the C_N^2 profile are: log-amplitude of light fluctuations, wave structure function, receiver diameter for heterodyne detection, and modulation transfer function.

In flight, the thermosonde passes its temperature difference measurement of $T_2 - T_1$ through a root mean square (rms) module. Ground-based processing converts this to the mean square temperature fluctuation $\overline{(T_2 - T_1)^2}$, which over one meter separation equals C_T^2. This is converted to C_N^2 through the equation:

$$C_N^2(h) = \left[\frac{79.9\ P(h) \times 10^{-6}}{T^2(h)}\right]^2 \times C_T^2 \qquad (1)$$

where P(h) is pressures in mbar and h is altitude.[1]

The original lightweight thermosonde system was developed by GTE Sylvania Inc., Electro-optics Organization for the Goddard Space Flight Center in 1971.[2,3]

1. Tatarski, V.I. (1961) Wave Propagation in a Turbulent Medium, McGraw-Hill Co., New York.

2. Titterton, P.J., Mallery, L.E., and Arken, T.A. (1971) Lightweight Thermosonde System, GTE Sylvania, Inc., Final Report, NAS5-11493.

3. GTE Sylvania, Inc. (1972) Lightweight Thermosonde System Model 140 (Instruction Manual), Mountain View, California, B440.

This prototype system was flown by the balloon branch of the AFCRL on 18 November 1971 at Chico, Calif. and the results were analyzed by Jack L. Bufton of the Goddard Space Flight Center, NASA.[4,5]

Modifications to improve the operation of this system were made in 1975 by the Air Force Weapons Laboratory, Kirtland AFB, N. Mex. with assistance of personnel from Dynalectron Corporation.[6] A new electronics board layout and component replacements were performed at AFGL in 1977. For the current 1981 program in which 50 thermosonde units were required, it was necessary to construct a completely new circuit board layout (Figure 2) with some design modifications. Tri-Con Associates, Inc. provided the design and layout schematics,[7] and the fifty units were assembled and tested by the engineering services section of the AFGL balloon branch.

3.1 Thermosonde Description

The thermosonde consists of two fine-wire tungsten probes exposed to the ambient atmosphere and separated by 1 m. Each probe has a resistance defined as $R_p = R_o + \alpha R_o(T-T_o)$. The temperature difference between the two probes, ΔT, is determined from an observed difference in resistance,

$$\Delta R_p = R_2 - R_1 = \alpha R_o \Delta T \quad , \tag{2}$$

where R_o is the resistance of the sensor at the point T_o. The two probes form elements of an ac Wheatstone bridge which is driven by a 30-kHz sinusoidal constant current source. Any resistance fluctuation in the bridge modulates the driving source, which is transformer coupled to a preamplifier. The signal is then passed through a demodulator, additional amplifiers, low and high pass filters, a trim module, and a current converter module. This current signal is used to drive the MHF data oscillator of the radiosonde package. After demodulation, a feedback loop supplies a sense voltage to a bridge balance restoring circuit. The bridge is electronically rebalanced with a time constant of 20 sec. Thus, dc resistance shifts due to temperature drifts are cancelled. The system bandwidth is set by a 4-pole Butterworth and low-pass filter network whose -3 dB cutoff frequencies are

4. Bufton, J.L. (1973) Correlation of microthermal turbulence data with meteorological soundings in the troposphere, J. Atmos. Sci. 30:83-87.
5. Bufton, J.L. (1975) A Radiosonde Thermal Sensor Technique for Measurement of Atmospheric Turbulence, NASA TN D-7867.
6. Curatolo, C. (1979) Modifications to GFD Sylvania Thermosonde for Improved Operation, Final Report, AFWL-TR-75-180, ADA 016227.
7. Murphy, G.P. (1981) New Techniques and Devices for Measuring Stratospheric Turbulence, AFGL-TR-81-0126, ADA 102680.

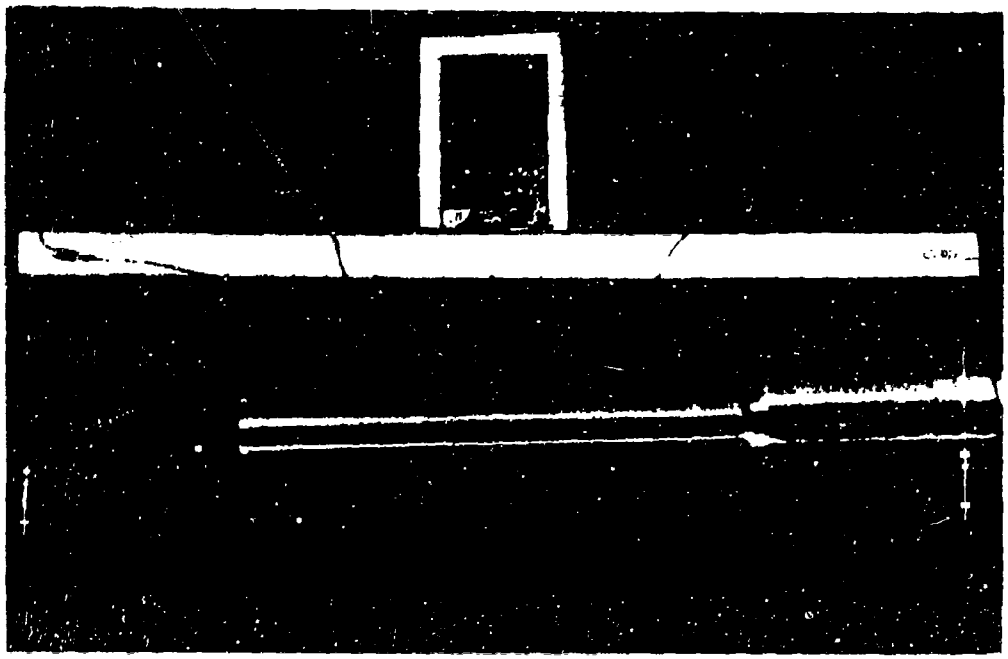

Figure 2. Photograph of Thermosonde and Micro Thermal Probe. Tungsten wire diameter 3.45 μm. Effective length is 0.45 cm. Nominal ice point resistance is 27 ohms and its temperature coefficient of resistance is $0.00375^{\circ}C^{-1}$. Sensor wire retouched for better photographing

1000 Hz and 0.2 Hz, respectively. A 1-sec rms average is performed on the filtered signal.

In the case of a square wave signal, the rms resistance is one-half the peak-to-peak resistance and Eq. (2) becomes

$$\Delta T_{rms} = \Delta R_p / (2 \alpha R_o) \quad . \tag{3}$$

The fine 99.98 percent pure tungsten wire is manufactured by the Sigmond Cohen Corp., Mt. Vernon, N.Y., and the wire is attached to a probe assembly by Datametrics, Inc. The nominal wire diameter is 3.45 μm. A 0.45-cm length of the wire is mounted between two 0.5-cm long wire supports extending out from the probe holder (Figure 2). Its nominal ice point resistance, R_o, is 27 ohms at $0^{\circ}C$. This sets the electrical resistivity at 5.9 μΩ - cm. The temperature coefficient of resistance was measured at $0.00375^{\circ}C^{-1}$. Note that the electrical

resistivity and temperature coefficient differ from tabulated values. This is probably due to a low annealing temperature of the drawn wire.[8]

3.2 Sensor Heating Effects

Optimum performance of the thermosonde can be achieved by passing a current through the wire that is large enough to enhance the temperature response, but small enough to avoid significant velocity response. Since a cool ambient fluid flowing over a warmer body will lower the temperature of the body toward the fluid temperature, it is desirable to keep the current-induced temperature difference below the minimum detectable value of 0.002^{o}C rms. The maximum current allowed for not exceeding this temperature difference can be estimated from a heat transfer analysis. The current generated temperature difference, ΔT_W, can be determined as

$$\Delta T_W = \frac{\Delta P}{J A_s h} \quad , \tag{4}$$

where

ΔP is the electrical power input between two conditions

J is the mechanical equivalent of heat 4.18 (Joule/Cal)

A_S is the surface area of the wire = 5×10^{-4} (cm^2)

h is the heat transfer coefficient (Cal $\cdot$ s^{-1} $\cdot$ cm^{-2} $\cdot$ $^{o}K^{-1}$).

The power input is $P = I^2(R_A + \Delta R)$ where R_A is the sensor resistance in the absence of an applied current and ΔR is the change in resistance due to applied current.

The heat transfer coefficient of the actual thermosonde probe was determined in the laboratory by the temperature difference between two power levels. A special bridge test circuit (Figure 3) was built to provide a constant current across the bridge. This current alternatively can be stepped high and low, depending upon the input voltage E. The bridge output, E_o, was amplified by a factor of 83.33. The additional wire resistance, R, caused by the current heating was determined from the observed voltages and current as

$$R = E_o / 83.33 I_i \quad . \tag{5}$$

The current converter input voltages were stepped from 0.5 V to 5 V, which produced probe currents, I_i, of 0.5 mA and 5 mA, respectively. The observed

8. Smithells, C.J. (1952) Tungsten, A Treatise on Its Metallurgy, Properties And Applications, Chapman & Hall, London, 3rd ed.

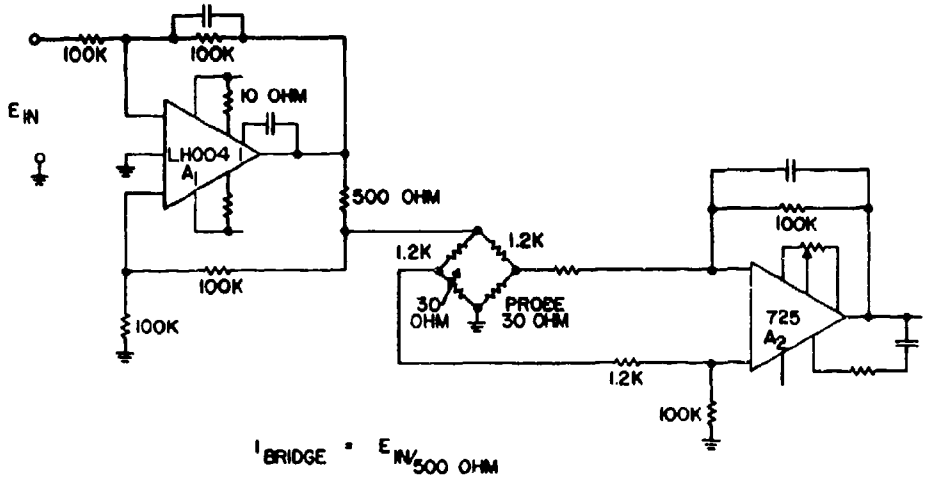

Figure 3. Schematic of Thermosonde Sensor Convective Heat Transfer Test Circuit. For a given input voltage, E_{in}, the LH0041 circuit produces a constant probe current of $(E_{in}/(2 \times 500))$ amps. The 725 amplifier provides an output, E_o = 83.33 × Bridge potential difference. Thus the differential resistance of the bridge due to probe I^2R heating is: $R = E_o/83.33\ I_i$

outputs were 0.01 V and 0.32 V. The temperature difference produced in the wire, ΔT_W, is

$$\Delta T_W = (R_{5.0} - R_{0.5})/\alpha R_o \ , \qquad (6)$$

where in this case R_o = 26.28 Ω, $\Delta R = R_{5.0} - R_{0.5}$ = 0.528 Ω, and $\Delta T_W = 5.36^oC$.

The difference in power between the two test conditions was determined as $\Delta P = P_{5.0} - P_{0.5} = (24.75\ R_A + 60\ E_{5.0} - 6E_{0.5})\ \mu W$ with a measured R_A = 28.25 Ω, ΔP = 718 μW. From Eq. (4), the experimentally determined heat transfer coefficient is found, $h = 0.064\ cal \cdot s^{-1} \cdot cm^{-2} \cdot {}^oK^{-1}$.

In flight, using a probe power of 1/3 μW rms produces a self-heating temperature rise [using Eq. (4)] of

$$\Delta T = 0.0025^oC\ (rms) \ .$$

Consequently, self-heating effects set the thermosonde noise level at 0.002^oC. The actual flight condition heat transfer coefficient depends upon air velocity and density. A study was performed to determine the convective heat transfer coefficient

as a function Reynolds number. The heat transfer coefficient h is described in terms of the Nusselt number Nu_d as $h = Nu_d k/d$, where k is the thermal conductivity of the air and d is the characteristic length. The Nusselt number can be calculated from the Reynolds number Re_d over limited regions.[9] Calibrations of h vs pressure and wind velocity were performed in a bell jar/blower vacuum system at conditions corresponding to the surface level, that is, p = 760 mmHg, T = 24°C, velocity = $5m \cdot s^{-1}$ (corresponding to the vertical balloon ascent rate) Re = 1.2; h is evaluated to be 0.12 cal $\cdot s^{-1} \cdot cm^{-2} \cdot {}^{o}K^{-1}$ or double the "no-wind" condition. At lower pressures, the bell jar density is correlated with the standard atmosphere to obtain altitude. An altitude profile of h is constructed from these calibrations (Figure 4). Above 29-km altitude molecular flow occurs. Here, the free molecular heat conductivity given by Dushman is used.[10] It is clear that an increase in velocity (Reynolds number) at standard conditions enhances the value of h and lowers self-heating even below the specified 0.002°C. At the maximum expected altitude of about 30 km, $h = 0.031$ cal $\cdot s^{-1} \cdot cm^{-2} \cdot {}^{o}K^{-1}$, and self-heating can be expected to approach a noise value of 0.005°C.

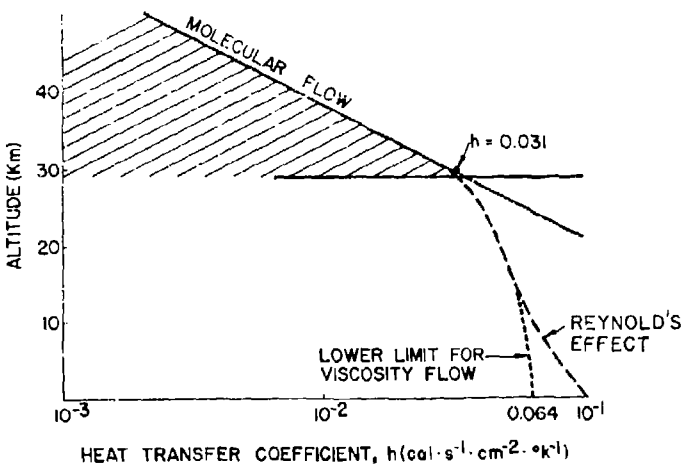

Figure 4. Heat Transfer Coefficient Curve of Thermosonde Sensor as a Function of Altitude. Bell jar calibration. At STP, h is measured at 0.064, cal $\cdot s^{-1} \cdot cm^{-2} \cdot {}^{o}K^{-1}$. With air speed = $5 m \cdot s^{-1}$, h = 0.12 cal $\cdot s^{-1} \cdot cm^{-2} \cdot {}^{o}K^{-1}$ at 30 km, h = 0.031 cal $\cdot s^{-1} \cdot cm^{-2} \cdot {}^{o}K^{-1}$. Above 30 km, free molecular conductivity applies

9. Marton, L. (1981) Fluid Dynamics, Academic Press, New York, Vol. 18, Part A, p. 271.

10. Dushman, S. (1962) Scientific Foundations of Vacuum Techniques, John Wiley, New York, p. 47, 2nd ed.

3.3 Sensor Frequency Response

If the temperature of the environment T_e suddenly changes, one wishes to know how fast the sensor will follow the environmental changes. Assume that the wire initially has a temperature T_i and is to be brought to an environment temperature T_e. The time for the wire temperature to recover a given fraction of the environmental temperature is given as:[11]

$$\frac{\theta_0}{\theta_i} = \frac{1 - 2\alpha bt}{r} \tag{7}$$

where,

$\theta_0 = T_{max} - T_e$

$\theta_i = T_i - T_e$

r = wire radius (cm)

α = thermal diffusivity of the wire (cm^2/sec)

$b = h/k$

h = convective heat transfer coefficient ($cal \cdot s^{-1} \cdot cm^{-2} \cdot {}^oK^{-1}$)

T_{max} = the maximum temperature in the wire after time, t

k = thermal conductivity of tungsten ($cal \cdot s^{-1} \cdot cm^{-1} \cdot {}^oK^{-1}$)

$= 0.426\ cal \cdot s^{-1} \cdot cm^{-1} \cdot {}^oK^{-1}$

$\alpha = k/(\rho_w C_{pw})$

ρ_w = tungsten density = $19.3\ g \cdot cm^{-3}$

C_{pw} = heat capacity of tungsten = $0.032\ cal \cdot g^{-1} \cdot {}^oK^{-1}$

$\alpha = 0.69\ cm^2 \cdot s^{-1}$

$b = 0.16\ cm^{-1}$

t = time (sec)

Thus, the response time required to recover θ_0/θ_i = 50 percent and θ_0/θ_i = 90 percent is 0.4 msec and 0.72 msec, respectively.

This was verified experimentally. The sensor was placed in a bell jar vacuum chamber. A current pulse train of 0.5- to 5- mA amplitudes was applied to the sensor and the ac bridge signal response was displayed on an oscilloscope. It was observed that the bridge output approached 1/2 of its full-scale change in 0.3 msec. This gives a frequency response $f_{1/2}$ = 3570 Hz. It is clear that the sensor has an adequate temperature frequency response for the purpose of turbulence measurements.

---

11. Jakob, M. (1949) Heat Transfer, John Wiley, New York, Vol. 1, p. 291.

3.4 Thermosonde Calibration

The thermosonde measurement is transmitted as a frequency value, nominally ranging between 30 and 700 Hz. Each frequency is related to a resistance which is defined by the observed temperature difference using Eq. (3). The relationship between frequency and resistance is determined by actual observations. A thermosonde test box was fabricated that alternately switches a test resistor in and out across one of the pair of matched 27 Ω resistors to simulate the probes. Any one of 12 precision resistors ranging from 1.4 MΩ to 20 kΩ can be inserted for the test resistor. These parallel resistors establish a known equivalent resistance. The differential resistance (ΔR) across the bridge is then,

$$\Delta R = R_{ps} - R_{eq}$$

where R_{ps} is the simulated probe resistor ≈ 27 Ω, and

$$R_{eq} = \frac{R_{ps} \times R_s}{R_{ps} + R_s}$$

where R_s is the inserted test resistor. Thus,

$$\Delta R = \frac{R^2_{ps}}{R_{ps} + R_s}$$

For each thermosonde a table is constructed for ΔR vs radiosonde frequency. ΔT_{rms} is calculated from Eq. (3) and a polynomial fit is performed on this data in order to provide the transfer function. Typical calibrations are shown in Figures 5 and 6.

3.5 Thermosonde Environment

The thermosonde was suspended 18 m below the sonde balloon. The balloon diameter expands from approximately 2 m at launch to about 10 m at 30 km.

A working rule is to locate experiments at least five diameters below the balloon to avoid wake effects. The 18-m suspension length is a compromise. A longer length can enhance a pendulum motion that would interfere with measurements. Thus, it is expected that the thermosonde will be located inside the balloon wake except during instances of large shears. However, even with the thermosonde inside the balloon wake, it is not clear what type of thermosonde error, if any, the wake would produce.

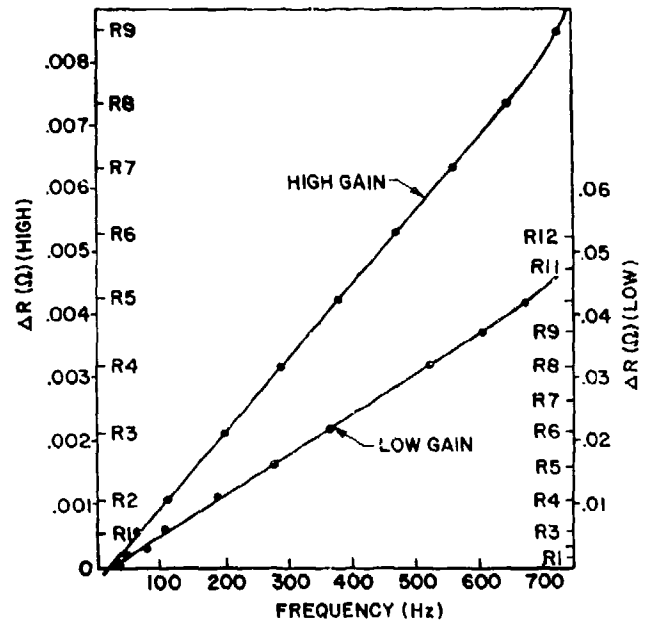

Figure 5. Calibration Curve of Thermosonde Sensor ΔR as a Function of Radiosonde Frequency. Test resistors are switched quickly across simulated probes. This provides a calibration frequency for each known differential resistance

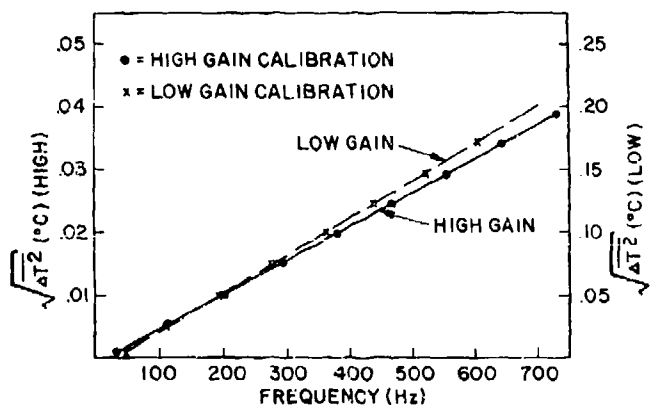

Figure 6. Calibration Curve of Thermosonde $(\Delta T)_{rms}$ as a Function of Radiosonde Frequency. For a probe of given resistance and temperature coefficient, the resistance vs frequency calibration curve is converted to $(\Delta T)_{rms}$ vs frequency

The existence of a wake behind a slow moving balloon (Re ~ 10^5) could generate a temperature fluctuation due to two mechanisms. The first is due to turbulent mixing of the atmospheric temperature structure over some vertical scale length. The second could arise as a companion to compressible flow fluctuations of the velocity in the wake.

In the troposphere, the sonde is usually in supercritical flow, and the separated flow produces organized vortices. At about 11-kms, the flow becomes subcritical and the flow around the balloon turns into a randomized separation and a uniform turbulent wake. Analysis of the thermosonde data reveals no significant differences between tropospheric and stratospheric data. The thermosonde data indicates the probability of C_T^2 is log normally distributed. Power spectral analysis of C_T^2 shows that no frequency spikes or features exist over the measurement range of 2- to 200-sec periods. This implies that any wake effects arising from atmospheric structure would have to arise from scales smaller than 10 m. The thermosonde observes layers of high C_T^2 over scales larger than 20 m as well as undetectable C_T^2 (S/N < 1) for scales larger than 10 m. This strongly suggests that the existence of a wake does not cause false signals.

The explanation of why there is no wake effect could be due to the rapid dissipation of wake gradients. The small scale of the wake (length less than 10 m) allows rapid mechanical mixing to a still smaller scale followed by rapid thermal dissipation. We have made measurements of the rate of energy dissipation, ε, in the wake of high altitude aircraft. Film density analysis of aircraft wakes marked by creating a smoke trail of titanium oxide hydrates shows the energy decay rate to follow a t^{-4} dependence. Thus, for a vertical rise rate of 5 m/sec, the balloon wake energy should be expected to dissipate to 1/256 of its original value by the time it reaches the thermosonde.

Confidence in the absence of wake effect will be developed as more of the data is analyzed and C_N^2 comparisons are made with the scintillometer and radar.

4. DATA REDUCTION

The "raw" transmitted MET signal is bandpass filtered at 400 Hz and 5000 Hz, after which it triggers a "one shot" comparator. This results in a "clean" train of constant-amplitude/constant-width pulses equivalent to the MET frequencies. A Hewlett-Packard model 5326b timer/counter measures the time period of every other frequency period and transfers these times in a binary coded decimal format to a Honeywell computer, model 316. The computer packs a magnetic tape eight bits per word in a pre-determined record size and format. These tapes are then unpacked and converted to CDC 6600 computer compatible 9 track tapes.

4.1 Time Period Records

Running time is determined by setting the algorithm time = Header time + $2\sum_{i=1}^{N} T_{true}$, where header time is the actual Zulu time at the start of each computer record. The factor 2 appears because the counter measures every other period. The true time period is:

$$T_{true} = \frac{\text{tape speed input to counter}}{\text{tape speed of original recording}} \times \text{measured counter time} .$$

For this series, the tape speed counter input was 1/2 the original tape speed. If any T_{true} is less than 0.91 msec, it is considered a data glitch and dropped from the summation and analysis.

4.2 Reference Frequency ID

The unpack routine is initialized to the measured reference frequency at launch. A forward test searches for three successive data periods with a frequency of the initialized value ±5 percent. When this criterion is achieved, a backwards test searches in reverse from the first of the three found frequencies to the first encounter of the initialized reference frequency ±50 Hz. Once aloft, the reference frequency is allowed to drift slowly from its initialized value.

4.3 Segment Window ID

After locating the last reference period of the previous reference segment, the time interval of the entire eight segment commutation frame is measured by summing each period and multiplying the result by two as described before. This defines the frame time. Since there are eight segments, the frame time is divided by eight to identify each segment interval. Since the frame rate is set at approximately 2.0 sec, the segment dwell time is approximately 250 msec per segment. Only the center 60 percent of each time segment is used in the frequency determination for that segment. The first and last 20 percent of the segment time is dropped and the remaining periods are averaged. Inverting the average period provides the average frequency for the segment. The standard deviation of each segment interval is calculated, and if σ_{ref} exceeds ± 10 Hz, or if σ_{temp}, σ_{RH}, or σ_{press} exceeds ± 5 Hz, the two smallest time periods are dropped. In most cases this removes spurious pulses. A new average and σ are redetermined, and if σ_{ref} exceeds ± 10 Hz, the entire commutation frame is dropped from analysis. If σ_{temp}, σ_{RH}, or σ_{press} exceeds ± 5 Hz, the calculated segment frequency is considered erroneous, and individual bad segments are dropped from analysis. In addition, if at least two time periods are not found in a particular segment, that segment is dropped from analysis. The segment sequence per frame is, in most cases:

reference, thermosonde high gain, temperature, relative humidity, thermosonde low gain, pressure, temperature, and relative humidity. When the thermosonde is not flown, those segments usually contain second samples of pressure and relative humidity.

4.4 Tracker Data

Due to the intrinsically low signal sensitivity of the on-board receiver, and to tracker hunting errors, large fluctuations occurred in the instantaneous position measurements of azimuth, elevation, and slant range. These data were refined after each flight on a CDC 6600 computer. The data, which were recorded every 0.1 sec, was edited by passing through a first difference software routine. Differences between adjacent points greater than two standard deviations from the average deviation were flagged. The average first difference is defined by:

$$\bar{e} = \sum_{i=2}^{n} \frac{(X_i - X_{i-1})}{n-1}$$

Where n is the number of points and X_i is the value of the ith point. The standard deviation is:

$$\sigma = \sqrt{\sum_{i=2}^{n} \frac{(X_i - X_{i-1})^2}{n-1} - \left[\frac{\sum_{i=2}^{n} (X_i - X_{i-1})}{n-1}\right]^2}$$

To smooth through the flagged data, a search was made to find four statistically acceptable points on either side of the flagged values. Once found, least squares polynomials were generated through this eight point array. Root-mean-square and Durbin-Watson criteria were used to automatically select the optimal fit, up to fifth degree. Polynomial interpolation then replaced the flagged data.

Smoothing of data within $\pm 2\ \sigma$ was performed by replacing centered data with a 3×3 moving average of neighboring points. The average is defined by:

$$X = 1/9X_{i-2} + 2/9X_{i-1} + 1/3X_i + 2/9X_{i+1} + 1/9X_{i+2} \ .$$

Simultaneously, a second arithmetic running average was performed on the resulting data to create 10-sec averages spaced at 2-sec intervals. Furthermore, the data went through a low-pass digital filter having a -3 dB band edge at 0.01 Hz that drops to -60 dB at 0.02 Hz.

The smoothed azimuth, elevation, and slant range were then transposed to X, Y, and Z Cartesian and geodetic coordinates. Using data time spacings of 30 sec, north, east, vertical, horizontal balloon speeds, and horizontal wind shears were calculated.

Sample results of the balloon position, velocity, and horizontal wind shear calculations are presented in Figure 7. The data are interpolated for even spacings of time every 2.0 second.*

5. PROGRAM DESCRIPTION

The general research objective of this program is to compare the measurements of atmospheric turbulence of several different experimental designs. The primary instruments consisted of the MIT Lincoln Laboratory 440 MHz[12] turbulence scatter radar and an Air Force Weapons Laboratory Stellar Scintillometer.[13] In addition to the primary instrumentation, radiosonde, thermosonde, and aircraft instrumentation were used to provide a broader comparison base. AFGL operated the sondes and scintillometer, while personnel from the Northeast Radio Observatory Corporation (NEROC) operated the radar. Aircraft measurements were provided by Airborne Research Associates, Bedford, Mass., under contract to AFGL.

From 10 Feb 1981 until 8 Aug 1981, over 30 radiosondes were flown. Twenty-nine of these are listed in Table 1. The preliminary qualification flights, up until 21 May 1981, were launched from AFGL. The remainder of the experiments (22) were launched near the NEROC Haystack Observatory at Millstone Hill, Westford, Mass., during the month of July.

Scheduling conflicts, time of day, and equipment availability dictated, to some extent, the particular experiment on a given day. The scintillometer could be operated only on cloudless nights. The aircraft required co-ordination with the FAA, and it was further constrained by bad weather and other scheduling difficulties. The radar was shared by other groups at Millstone, and it was available for these measurements only on those dates pre-arranged weeks in advance. The radiosonde

*As of this printing, a detailed description of the positional data was being prepared for publication as an AFGL technical memorandum. The title is: Analysis of Balloon Trajectory for the Calculation of Wind Velocities and Shears, by Sullivan, B., et. al.

12. Watkins, B.J. (1981) Millstone Hill Doppler Radar Observations of Winds and Turbulence, Middle Atmospheric Program, Handbook for MAP, Extended abstracts from Int. Sym. on Middle Atm. Dyn. 2:30-36.

13. Ochs, G.R., Lawrence, R.S., and Wang, T. (1976) Stellar scintillation measurement of the vertical profile of refractive-index turbulence in the atmosphere, Proc. Soc. of Photo-optical Inst. Eng. 75:48-54.

HR	MIN	SEC	UTSEC	ALT	GRANGE	SRANGE	ELV	AZIM	LAT	WLONG	E	N	HDIR	VE	VN	VZ	VHOR	SHOR
QX0020			11/23/81	(KM MSL)	(KM)	(KM)	(DEG)	(DEG)	(DEG)	(DEG)	(KM)	(KM)	(DEG)	M/SEC	M/SEC	M/SEC	M/SEC	1./SEC
2	19	17.0	8357.0	15.02	55.77	58.02	14.72	118.52	42.21	70.92	48.85	-26.90	99.21	17.23	-2.79	5.18	17.45	.02496
2	19	19.0	8359.0	15.03	55.80	58.05	14.73	118.51	42.21	70.92	48.88	-26.91	98.77	17.50	-2.70	5.20	17.71	.02358
2	19	21.0	8361.0	15.04	55.83	58.09	14.73	118.50	42.21	70.92	48.92	-26.91	98.39	17.76	-2.62	5.23	17.95	.02193
2	19	23.0	8363.0	15.05	55.87	58.12	14.73	118.48	42.21	70.91	48.95	-26.92	98.05	17.99	-2.55	5.24	18.17	.02005
2	19	25.0	8365.0	15.06	55.90	58.16	14.73	118.47	42.21	70.91	48.99	-26.92	97.78	18.21	-2.49	5.25	18.38	.01802
2	19	27.0	8367.0	15.07	55.94	58.19	14.73	118.45	42.21	70.91	49.03	-26.93	97.59	18.40	-2.45	5.25	18.56	.01590
2	19	29.0	8369.0	15.09	55.97	58.23	14.73	118.44	42.21	70.91	49.07	-26.93	97.47	18.56	-2.43	5.24	18.72	.01384
2	19	31.0	8371.0	15.10	56.01	58.27	14.73	118.42	42.21	70.91	49.10	-26.93	97.43	18.70	-2.44	5.22	18.86	.01201
2	19	33.0	8373.0	15.11	56.04	58.31	14.73	118.41	42.21	70.91	49.14	-26.94	97.48	18.81	-2.47	5.20	18.97	.01068
2	19	35.0	8375.0	15.12	56.08	58.34	14.73	118.40	42.21	70.91	49.18	-26.94	97.61	18.89	-2.52	5.17	19.08	.01014
2	19	37.0	8377.0	15.13	56.11	58.38	14.73	118.38	42.21	70.91	49.22	-26.95	97.83	18.95	-2.61	5.12	19.13	.01056
2	19	39.0	8379.0	15.14	56.15	58.42	14.73	118.37	42.21	70.91	49.26	-26.95	98.14	18.98	-2.72	5.08	19.17	.01180
2	19	41.0	8381.0	15.15	56.19	58.46	14.73	118.35	42.21	70.91	49.30	-26.96	98.54	18.99	-2.85	5.02	19.20	.01360
2	19	43.0	8383.0	15.16	56.22	58.49	14.73	118.34	42.21	70.91	49.33	-26.96	99.01	18.97	-3.01	4.97	19.21	.01567
2	19	45.0	8385.0	15.17	56.26	58.53	14.73	118.32	42.21	70.91	49.37	-26.97	99.56	18.94	-3.19	4.90	19.21	.01781
2	19	47.0	8387.0	15.18	56.29	58.57	14.73	118.31	42.21	70.91	49.41	-26.98	100.18	18.89	-3.39	4.84	19.19	.01991
2	19	49.0	8389.0	15.19	56.33	58.61	14.73	118.30	42.21	70.91	49.45	-26.98	100.86	18.83	-3.61	4.77	19.18	.02186
2	19	51.0	8391.0	15.20	56.37	58.65	14.73	118.29	42.21	70.91	49.49	-26.99	101.59	18.77	-3.85	4.69	19.16	.02360
2	19	53.0	8393.0	15.21	56.40	58.68	14.73	118.27	42.21	70.91	49.52	-27.00	102.35	18.70	-4.09	4.62	19.14	.02508
2	19	55.0	8395.0	15.22	56.44	58.72	14.73	118.26	42.21	70.91	49.56	-27.01	103.15	18.62	-4.35	4.54	19.13	.02629
2	19	57.0	8397.0	15.22	56.48	58.76	14.73	118.25	42.21	70.91	49.60	-27.01	103.96	18.55	-4.61	4.47	19.12	.02719
2	19	59.0	8399.0	15.23	56.51	58.80	14.73	118.24	42.21	70.91	49.63	-27.02	104.77	18.49	-4.87	4.40	19.12	.02779
2	20	1.0	8401.0	15.24	56.55	58.84	14.73	118.24	42.21	70.91	49.67	-27.03	105.57	18.43	-5.14	4.32	19.13	.02808
2	20	3.0	8403.0	15.25	56.59	58.88	14.73	118.23	42.21	70.91	49.71	-27.04	106.36	18.38	-5.39	4.25	19.15	.02807
2	20	5.0	8405.0	15.26	56.63	58.91	14.73	118.22	42.21	70.91	49.74	-27.06	107.12	18.34	-5.65	4.18	19.19	.02779
2	20	7.0	8407.0	15.27	56.66	58.95	14.72	118.21	42.21	70.90	49.78	-27.07	107.84	18.31	-5.89	4.11	19.23	.02724
2	20	9.0	8409.0	15.28	56.70	58.99	14.72	118.20	42.21	70.90	49.82	-27.08	108.51	18.29	-6.12	4.05	19.29	.02646
2	20	11.0	8411.0	15.28	56.74	59.03	14.72	118.20	42.21	70.90	49.85	-27.09	109.13	18.28	-6.34	3.99	19.35	.02547
2	20	13.0	8413.0	15.29	56.78	59.07	14.72	118.19	42.21	70.90	49.89	-27.11	109.70	18.28	-6.55	3.93	19.42	.02431
2	20	15.0	8415.0	15.30	56.82	59.11	14.71	118.19	42.21	70.90	49.93	-27.12	110.22	18.29	-6.74	3.88	19.50	.02298
2	20	17.0	8417.0	15.31	56.85	59.15	14.71	118.18	42.21	70.90	49.96	-27.13	110.68	18.31	-8.91	3.84	19.57	.02154
2	20	19.0	8419.0	15.31	56.89	59.19	14.71	118.18	42.21	70.90	50.00	-27.15	111.09	18.33	-7.07	3.80	19.65	.01999
2	20	21.0	8421.0	15.32	56.93	59.23	14.71	118.17	42.21	70.90	50.04	-27.16	111.45	18.36	-7.21	3.78	19.73	.01838
2	20	23.0	8423.0	15.33	56.97	59.27	14.70	118.17	42.21	70.90	50.07	-27.18	111.76	18.38	-7.34	3.74	19.79	.01674
2	20	25.0	8425.0	15.34	57.01	59.31	14.70	118.16	42.21	70.90	50.11	-27.19	112.04	18.40	-7.45	3.72	19.86	.01512
2	20	27.0	8427.0	15.34	57.05	59.35	14.70	118.16	42.21	70.90	50.15	-27.21	112.29	18.42	-7.55	3.71	19.91	.01362
2	20	29.0	8429.0	15.35	57.09	59.39	14.69	118.15	42.21	70.90	50.18	-27.22	112.51	18.43	-7.63	3.71	19.94	.01232
2	20	31.0	8431.0	15.36	57.13	59.43	14.69	118.15	42.21	70.90	50.22	-27.24	112.71	18.42	-7.71	3.72	19.97	.01138
2	20	33.0	8433.0	15.37	57.17	59.47	14.69	118.15	42.21	70.90	50.26	-27.25	112.90	18.40	-7.77	3.74	19.97	.01092
2	20	35.0	8435.0	15.37	57.21	59.51	14.68	118.14	42.21	70.90	50.29	-27.27	113.08	18.37	-7.83	3.77	19.98	.01102
2	20	37.0	8437.0	15.38	57.25	59.56	14.69	118.14	42.21	70.90	50.33	-27.29	113.26	18.32	-7.87	3.81	19.94	.01163
2	20	39.0	8439.0	15.39	57.29	59.60	14.68	118.13	42.21	70.90	50.37	-27.30	113.46	18.25	-7.92	3.86	19.89	.01264
2	20	41.0	8441.0	15.39	57.33	59.64	14.67	118.13	42.21	70.90	50.41	-27.32	113.66	18.18	-7.98	3.92	19.82	.01387
2	20	43.0	8443.0	15.40	57.37	59.68	14.67	118.13	42.21	70.90	50.44	-27.33	113.89	18.05	-7.99	3.99	19.74	.01518
2	20	45.0	8445.0	15.41	57.41	59.72	14.67	118.12	42.21	70.90	50.48	-27.35	114.14	17.93	-8.03	4.06	19.64	.01648
2	20	47.0	8447.0	15.42	57.45	59.78	14.66	118.12	42.21	70.90	50.51	-27.37	114.42	17.78	-8.07	4.15	19.53	.01764
2	20	49.0	8449.0	15.43	57.49	59.80	14.66	118.12	42.21	70.90	50.55	-27.38	114.73	17.63	-8.12	4.23	19.41	.01866
2	20	51.0	8451.0	15.44	57.53	59.84	14.66	118.11	42.21	70.90	50.59	-27.40	115.07	17.46	-8.17	4.32	19.27	.01950
2	20	53.0	8453.0	15.44	57.57	59.88	14.66	118.11	42.21	70.89	50.62	-27.41	115.45	17.28	-8.22	4.42	19.13	.02015
2	20	55.0	8455.0	15.45	57.60	59.92	14.66	118.11	42.21	70.89	50.65	-27.43	115.87	17.09	-8.29	4.51	18.99	.02060

Figure 7. Sample Output of Reduced Tracker Data. Edited and filtered

Table 1. Optical C_N^2 (Turbulence) Measurement Program

SOUND-ING #	RADIO-SONDE S/N	LAUNCH DATE (ZULU)	LAUNCH TIME (ZULU)	RADAR	SCINT-ILLO-METER	THER-MO-SONDE	AIR-CRAFT	BALLOON BURST (ZULU)	TAPE OFF (ZULU)	SITE	MAX HGT KM	REMARKS
1	NONE	Feb-10-81 not processed	20:14:45	-	-	-	-	?	21:59:45	GL	?	resistive commutator Press unknown
2	QX0018	Mar-19-81 not processed	?	-	-	x	-	?	?	GL	.03	Free fell at launch. Reflown APR-29-81
3	QX0021	Mar-23-81	18:49:55	-	-	x	-	?	20:25:00	GL	?	No station max No reel down. No wind anal.
4	QX0018	Apr-29-81	17:30:50	Radar x Invalid	-	-	-	19:22:30	19:32:00	GL	34.1	Auto-track 17:33:40 No Met Data.
5	QX0024	May-15-81	18:00:00 approx.	-	-	x	-	?	19:34:25	GL	?	
6	QX0026	May-19-81	18:40:36	-	-	x	-	?	19:50:00	GL	?	Auto-track 18:41:21
7	QX0009	May-21-81	17:29:50	x	-	-	-	19:12:50	19:29:05	GL	33.9	
8	QX0048	Jun-09-81	19:15:35	-	-	-	-	20:57:50	21:01:30	HAY	36.5	Auto-track 19:18:40
9	QX0050	Jun-30-81	22:37:32	x	-	x	-	00:27:50	00:35:05	HAY	35.5	Auto-track 22:37:32
10	QX0001	Jul-01-81	02:09:36	x	-	-	-	?	03:55:08	HAY	?	Winds not processed.
11	QX0005	Jul-09-81	01:30:28	x	-	x	-	03:15:30	?	HAY	33.6	Auto-track 01:42:10. Wind not processed.
12	QX0006	Jul-10-81	01:37:32	x	-	x	-	?	03:32:23	HAY	?	Auto track 01:38:09. Flown after T'Storm

Table 1. Optical C_N^2 (Turbulence) Measurement Program (Continued)

SOUNDING #	RADIOSONDE S/N	LAUNCH DATE (ZULU)	LAUNCH TIME (ZULU)	RADAR	SCINTILLOMETER	THERMOSONDE	AIRCRAFT	BALLOON BURST (ZULU)	TAPE OFF (ZULU)	SITE	MAX HGT KM	REMARKS
13	QX0005	Jul-11-81	20:33:05	x	-	-	x	22:15:00	22:30:07	Hay	35.3	Auto-track 20:33:32
14	QX0045	Jul-12-81	01:15:32	x	-	x	x	?	02:51:56	Hay	?	Auto-track 01:16:11
15	QX0007	Jul-15-81	02:28:27	-	x	-	-	?	03:41:00	Hay	?	Auto-track 02:28:59
16	QX0030	Jul-15-81	22:30:12	Radar x failure	-	x	x	?	?	Hay	?	No slant range No winds. Poor time code.
17	QX0046	Jul-17-81	01:50:45	x	-	x	x	03:10:20	?	Hay	33.3	Reel stuck - 15ft. Auto trk. 01:51:18
18	QX0036	Jul-23-81	01:37:13	-	x	x	-	?	03:23:03	Hay	?	Auto-track 01:39:40
19	QX0012	Jul-23-81	20:45:05	x	-	x	-	22:40:20	22:40:37	Hay	34.1	Auto-track 20:45:09
20	QX0034	Jul-23-81	? not processed	x	-	x	-	?	?	Hay	.03	Balloon burst Reflown Jul-30-81
21	QX0019	Jul-24-81	02:35:26	x	-	-	x	?	03:49:06	Hay	?	Auto-track 02:36:49
22	QX0038	Jul-25-81	20:44:19	Poor x Quality	-	x	-	22:43:10	22:43:20	Hay	34.8	Auto-track 20:44:20
23	QX0035	Jul-28-81	20:41:42	x	-	x	-	22:23:40	22:43:20	Hay	34.2	Auto-track 20:42:10
24	QX0043	Jul-29-81	21:41:18	x	-	x	-	23:15:00	23:40:10	Hay	33.2	Auto-track 21:41:38

Table 1. Optical C_N^2 (Turbulence) Measurement Program (Continued)

SOUND-ING #	RADIO-SONDE S/N	LAUNCH DATE (ZULU)	LAUNCH TIME (ZULU)	RADAR	SCINT-ILLO-METER	TEMP-SONDE	AIR-CRAFT	BALLOON BURST (ZULU)	TAPE OFF (ZULU)	SITE	MAX HGT KM	REMARKS
25	QX0011	Jul-30-81	01:12:47	x	-	x	-	?	02:40:00	Hav	?	Auto-track 01:13:03
26	QX0034	Jul-30-81	20:15:36	x	-	x	-	21:53:40	22:12:00	Hav	32.8	Auto-track 20:16:13
27	QX0020	Jul-31-81	01:28:12	x	x	x	-	03:33:30	03:22:52	Hav	35.1	Auto-track 01:30:30
28	QX0040	Aug-07-81	03:30:50	-	x	x	-	?	05:06:00	Hav	?	Auto-track 03:31:30
29	QX0031	Aug-08-81	05:49:34	-	-	x	-	07:36:50	07:45:39	Hav	28.1	Auto-track 05:49:50

and thermosonde had no constraints other than availability of tracking personnel. As it turned out, the scintillometer and radar operated together only on one evening, 31 July 1981. Good quality experiments using three techniques, radar, thermosonde, and aircraft were accomplished twice. Good quality radar and radiosonde measurements were completed on fifteen occasions. Good quality radiosonde and thermosonde experiments were operated on eighteen occasions. Radar, radiosonde, and thermosonde operated successfully on eleven occasions.

6. RESULTS

Results of typical experimental runs are presented in the following plots. Figures 8 and 9 show temperature and relative humidity profiles obtained 31 July. A small temperature inversion is found at 3 km that roughly corresponds with a high negative gradient in relative humidity. A more pronounced temperature inversion is found at 12 km, defining the tropopause.

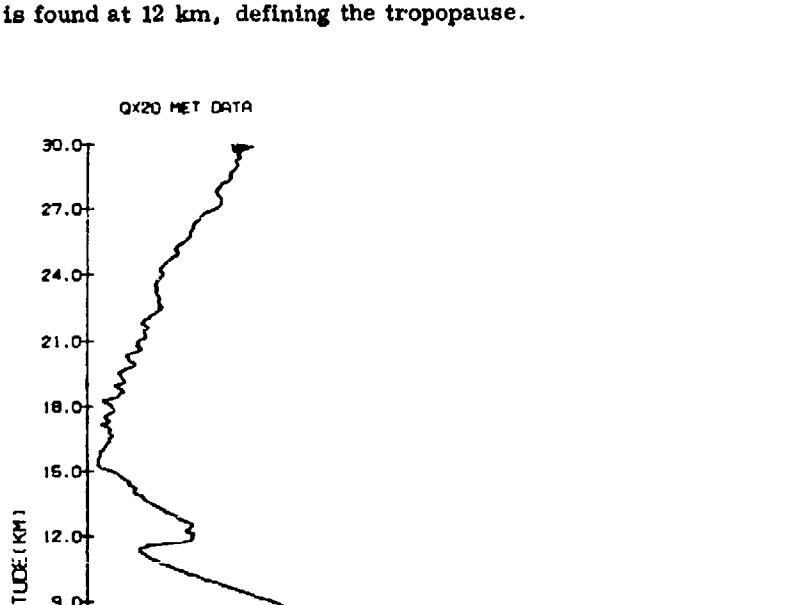

Figure 8. Typical Temperature Profile Plot. Processed result

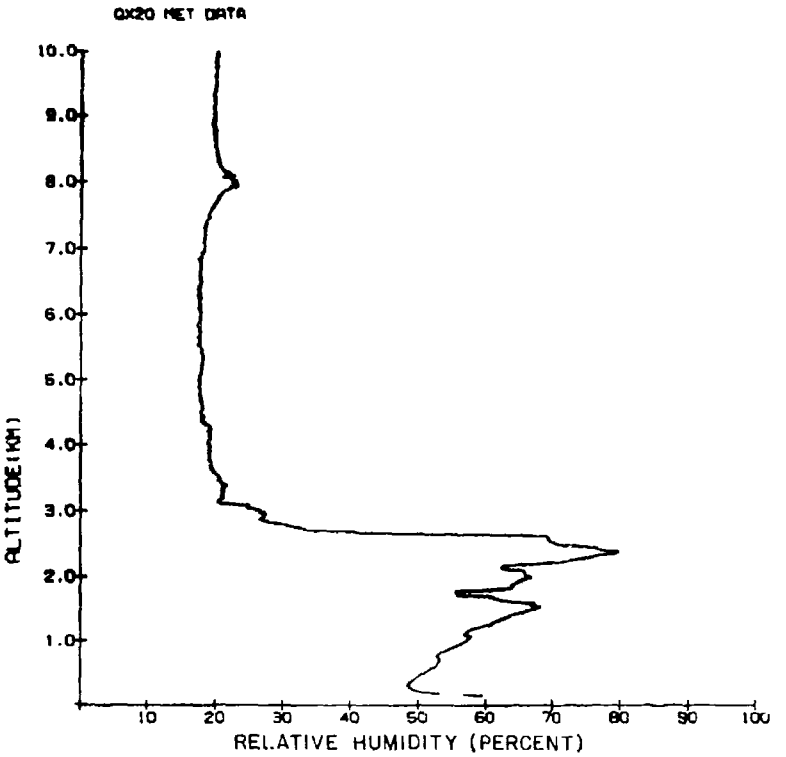

Figure 9. Typical Relative Humidity Profile Plot. Processed result

Figures 10 and 11 show the east and north balloon velocity component profiles. The maximum horizontal wind occurs at 10.7 km at 35 m/sec. The detailed wind structure is clearly evident.

Figure 12 shows the horizontal vector wind shear, S_H, profile to 30 km. S_H is defined as the resultant of the east and north horizontal component shears, or $S_H^2 = S_N^2 + S_E^2$. Figure 13 is an expanded view of Figure 12 in the altitude range from 20 km to 25 km and shows the mean shear at about 0.02 sec^{-1}. This plot shows structuring of the wind shear down to the spatial filter wavelength of about 120 m. The power spectral density of the winds are plotted in Figure 14. The slope is about -2.5, which compares well with other measurements.[14]

---

14. Endlich, R.M., and Singleton, R.C. (1969) Spectral analysis of detailed vertical wind speeds profiles, J. Atmos. Sci. 26:1030-1041.

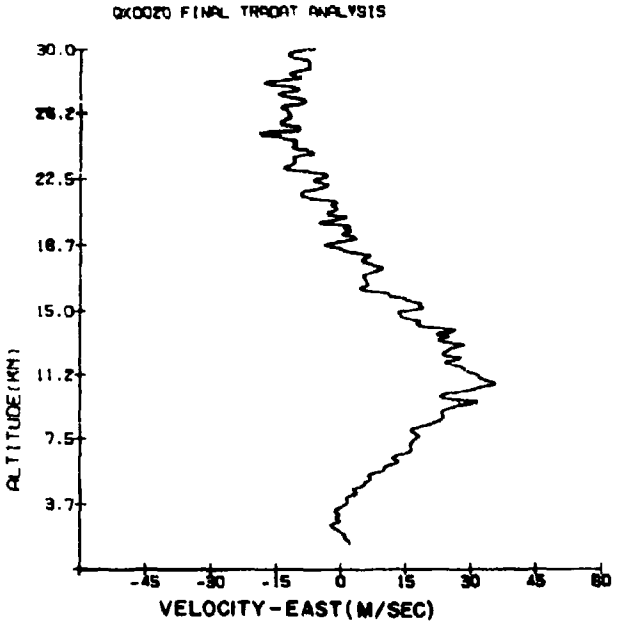

Figure 10. Typical Balloon Velocity Analysis – East Profile Plot. Edited and filtered

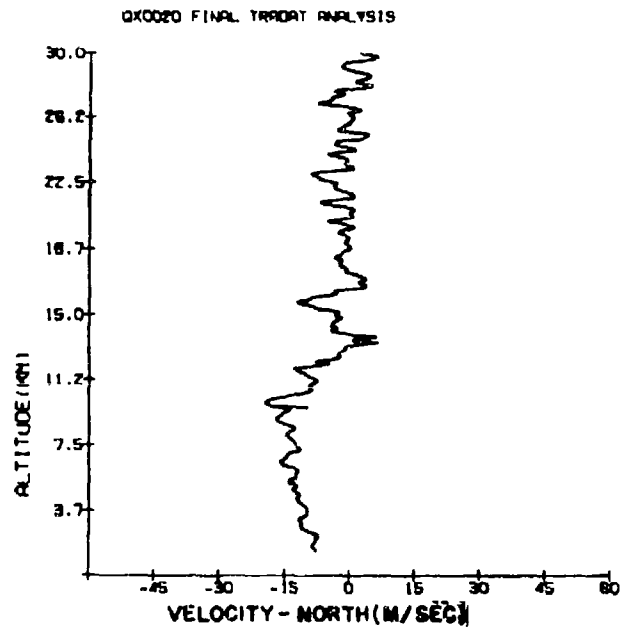

Figure 11. Typical Balloon Velocity Analysis – North Profile Plot. Edited and filtered

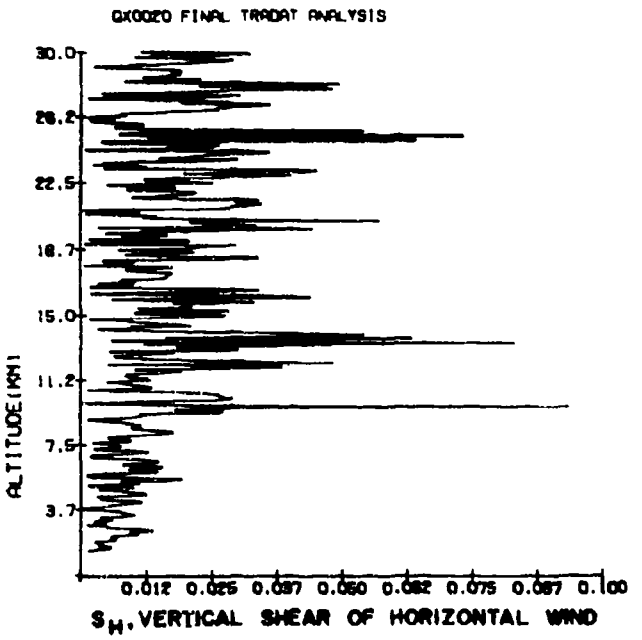

Figure 12. Typical Horizontal Vector Shear Analysis. Profile plot. Shear is calculated over a 30-sec data spacing

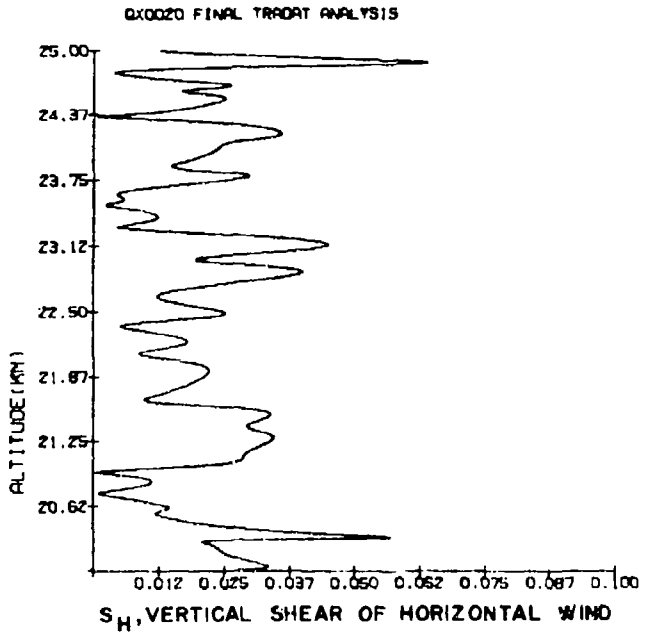

Figure 13. Expanded View of Horizontal Vector Shear. The shear altitude resolution is about 120 m

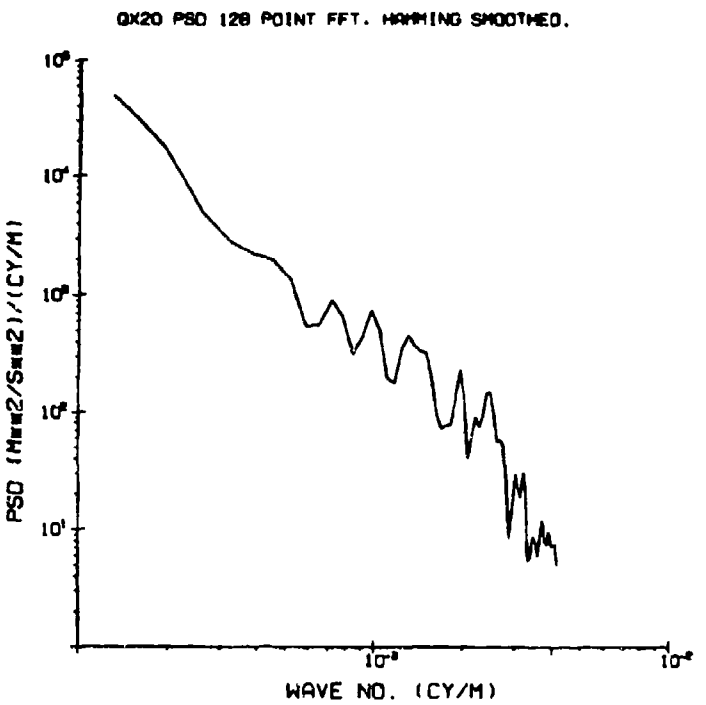

Figure 14. Power Spectral Density Analysis of Horizontal Vector Shear. The slope is about -2.5

Figure 15 shows "RAW" thermosonde C_N^2 values as a function of altitude. The mean C_N^2 tends to decrease logarithmically with altitude. Figure 16 is an expanded view of Figure 15 in the altitude range from 10 km to 15 km. A large-scale maximum shows up at 11.5 km while the fluctuations in C_N^2 appear to be due to the small sampling interval. C_N^2 smoothed to 120 m is plotted in Figure 17 for comparison. Figure 18 plots the cumulative frequency distribution of C_T^2. The data follows a straight line, except at the endpoints, which confirms the log normal distribution of C_N^2.

The purpose of the optical turbulence program was to compare various techniques of observing C_N^2. Sonde measurements were important in the low altitude comparison between radar, scintillometer, and thermosonde. The radar-received power, scattered by refractive index fluctuations, can be related to a C_N^2. This C_N^2 is caused by turbulent fluctuations in both temperature and water vapor concentrations. As the comparisons are based on optical wavelength C_N^2, the contribution of water vapor must be removed from the radar C_N^2.

The fluctuations of the refractive index across a layer is given[1, 15] as:

$$M = -77.6 \times 10^{-6} \frac{P\omega_B^2}{Tg} \left[1 + 15,500 \frac{q}{T} - \frac{15,500}{2} \frac{g}{T} \frac{q'}{\omega_B^2} \right] \quad (8)$$

where

P = pressure (mb)
T = temperature (Kelvin)
g = gravity ($m \cdot s^{-2}$)
q = specific humidity (gm/gm)
ω_B^2 = squared Brunt-Vaisala frequency (s^{-2}) = $(g/\theta)\theta'$
q' = vertical gradient of specific humidity (m^{-1})
θ' = vertical gradient of potential temperature (Kelvin/m)

The radar C_N^2 can be corrected to dry conditions, C_N^2 (dry) by evaluating the bracketed terms in Eq. (8) on the basis of the sonde measurements of P, T, and q.

$$C_N^2(\text{dry}) = C_N^2(\text{radar}) \frac{1}{\left[1 + 15,000 \frac{q}{T} - \frac{15,500}{2} \frac{g}{T} \frac{q'}{\omega_B^2} \right]^2}$$

The comparison between the C_N^2 (dry) derived from radar measurements and the optical scintillometer is shown in Figure 19. The optical scintillometer[13] obtains data over very large weighting functions. The scintillometer 1/e half-width varies from 1.4 km at an altitude of 2.2 to 4.9 km at an altitude of 14 km. The weighting functions are shown in Figure 20. The comparison between radar and scintillometer shown in Figure 19 is obtained by passing the C_N^2 (dry) through the six weighting functions.

A comparison of thermosonde data and the scintillometer is shown in Figure 21. Here the thermosonde data shown in Figure 15 is passed through the scintillometer weighting functions. This agreement is good. The large smoothing of the weighting functions hides whatever variations may exist due to the space and time differences in the respective measurements. The scintillometer viewed the sky vertically while the thermosonde followed a slant path.

Thermosonde and radar comparison can be made over very nearly the same volume and space by the fact that the radar can be pointed in the direction of the sonde. The radar C_N^2 (dry) is obtained over one-minute periods and averaged over

---

15. VanZandt, T.E., Gage, K.S., and Warnock, J.M. (1981) An Improved Model for the Calculation of Profiles of C_N^2 and ϵ in the Free Atmosphere from Background Profiles of Wind, Temperature, and Humidity, 20th conf. on Radar Meteorology, (30 Nov–3 Dec 1981).

five minutes. A composite of the radar results is made to match the sonde altitude and times. The comparison of radar and thermosonde C_N^2 values is presented in Figure 22. The thermosonde data has been averaged over 0.50-km intervals.

The comparisons shown indicate the thermosonde radar and scintillometer are in quite good agreement. The data shown represents the results from just one day's measurements. Detailed comparisons involving all the data sets will be analyzed and presented in separate scientific reports.

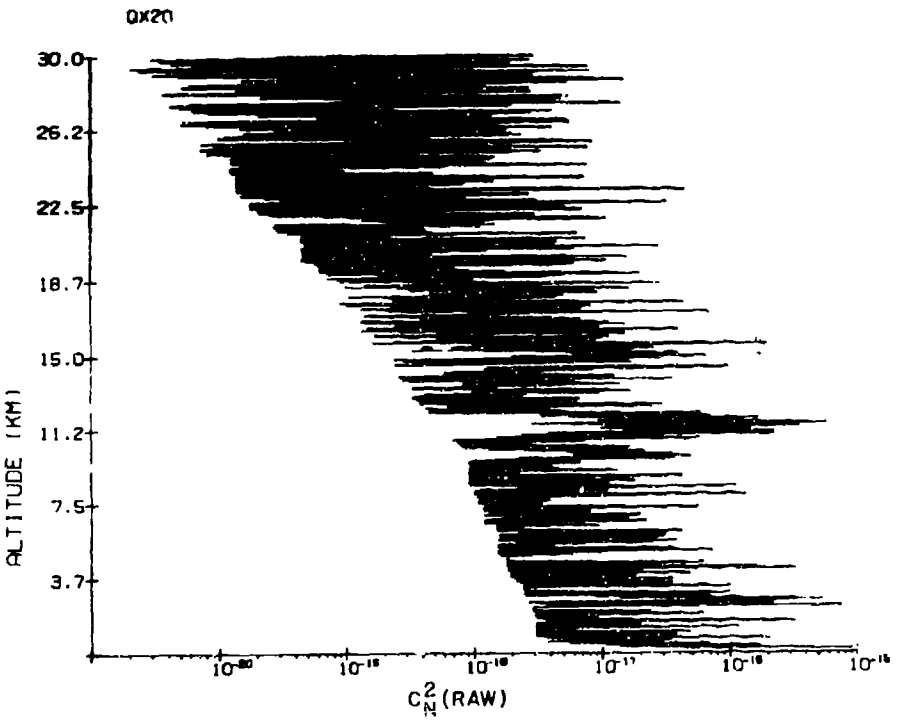

Figure 15. Raw Thermosonde C_N^2 Analysis – Profile Plot. Low and high gain measurements have been combined into a single best measurement. The thermosonde measures C_N^2 from ground level to 30 km. C_N^2 is calculated from C_N^2 and the radiosonde measurements of pressure and temperature

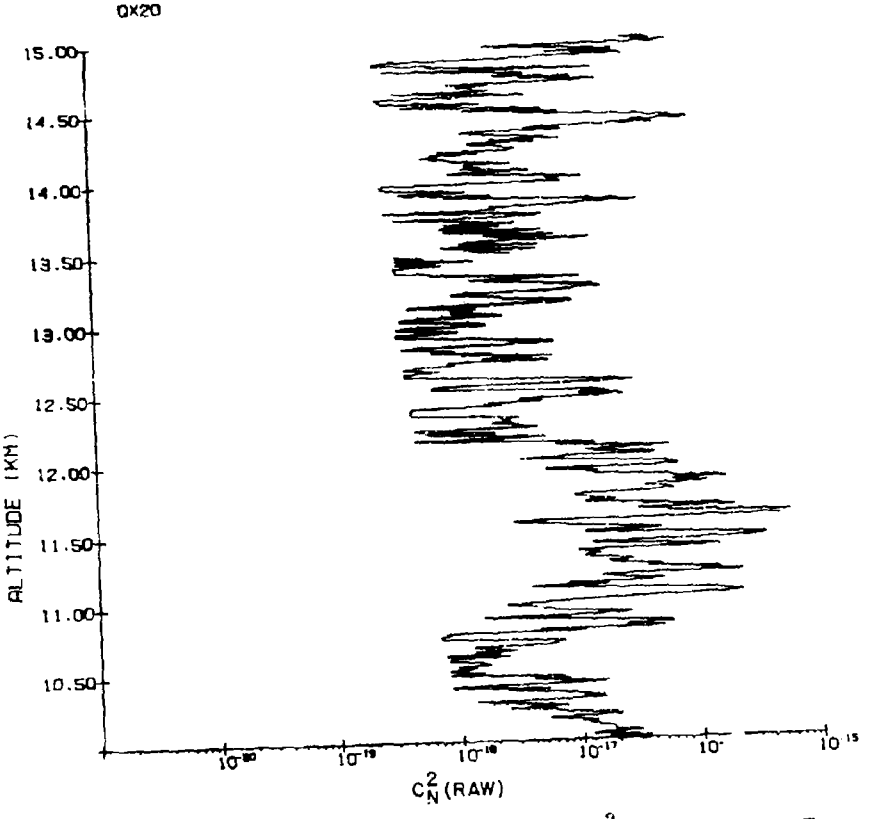

Figure 16. Expanded View of Raw Thermosonde C_N^2 Profile Plot. The altitude resolution of C_N^2 is about 10 m. Each data point is a result of the rms value of C_T taken over 1 sec

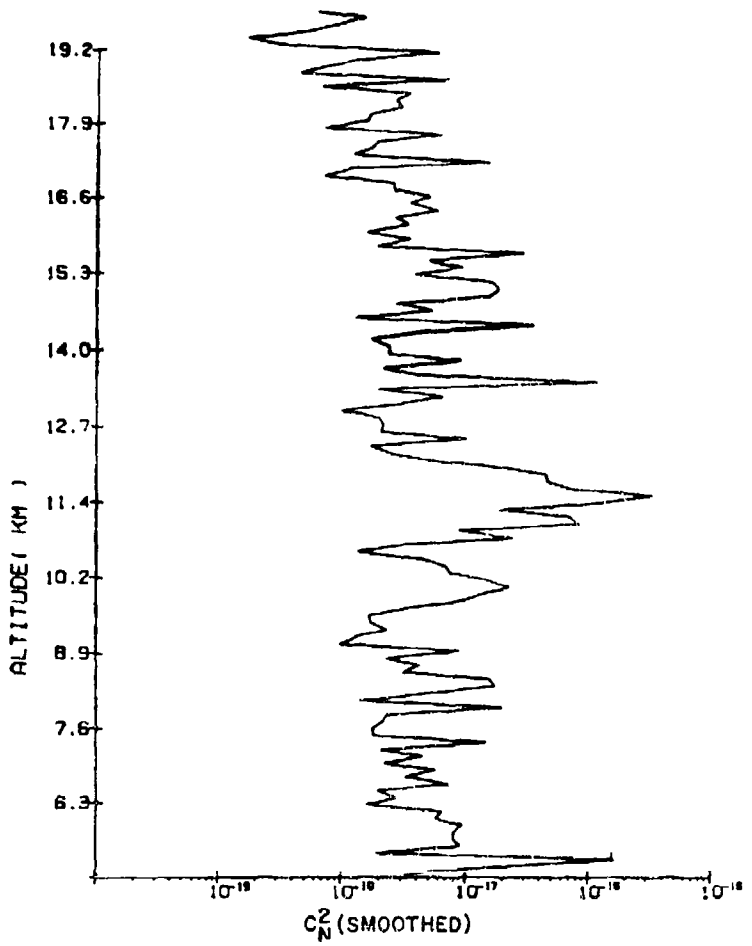

Figure 17. Smoothed Thermosonde C_N^2 Profile Plot. C_N^2 is smoothed over 120 m

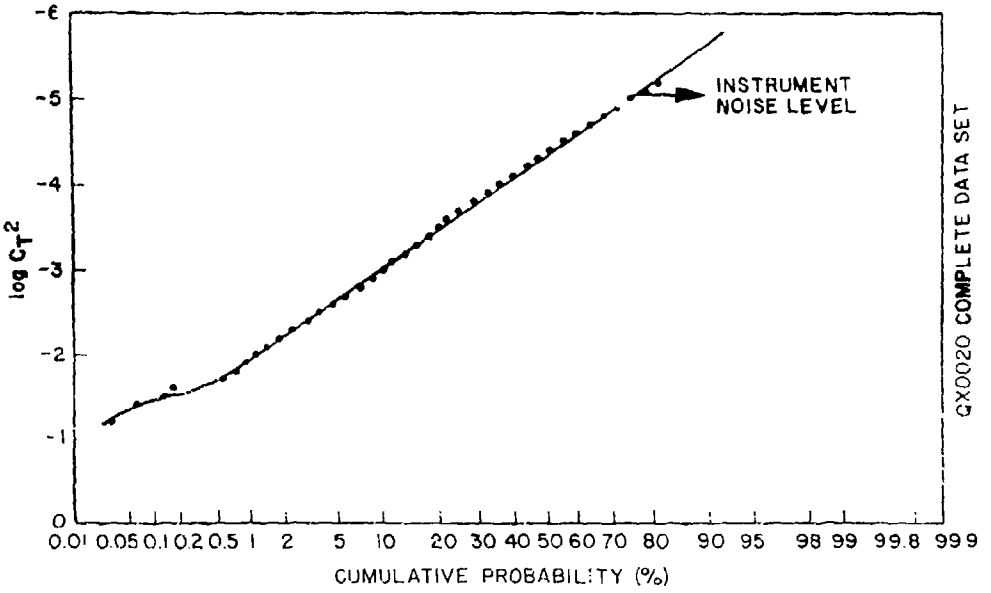

Figure 18. Cumulative Probability Distribution Curve of LOG C_T^2. Thermosonde C_N^2 shows a log normal distribution. For this data set the 50 percent probability C_T^2 is 4.5×10^{-5} $^{o}C^2$

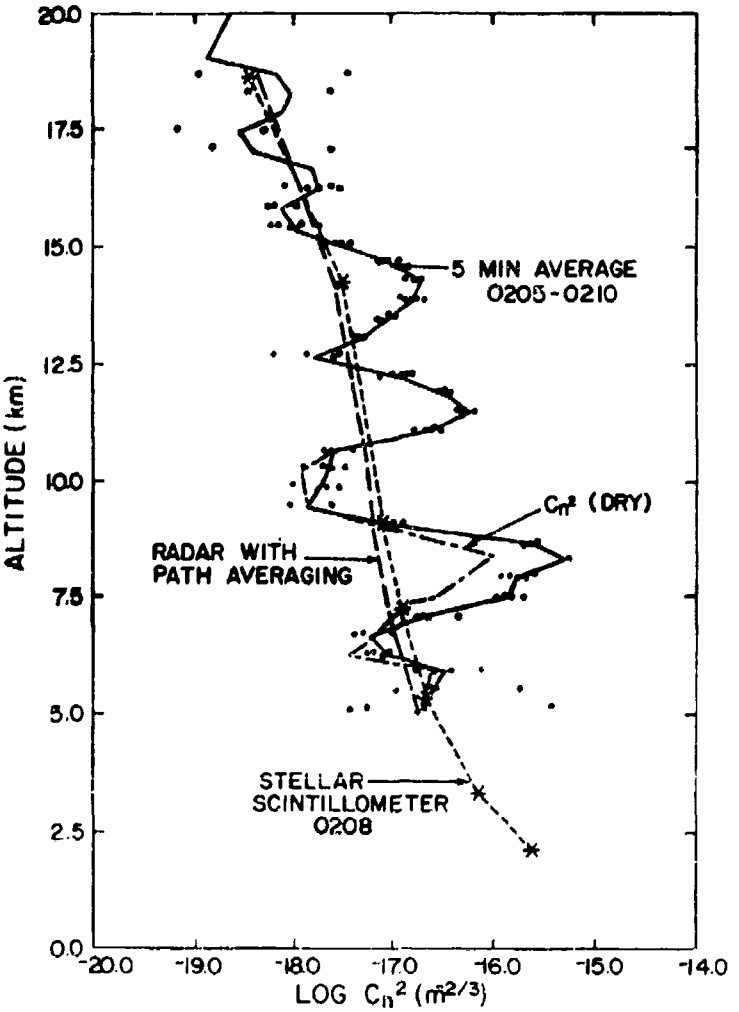

Figure 19. Comparison of Radar C_N^2 and Scintillometer C_N^2 Profiles. The path averaged radar and scintillometer profiles show good agreement. The points depict radar C_N^2 measurements. The solid line through the radar points represent 5-min radar averages. The seven scintillometer measurements are shown as * with straight lines drawn between them. The dashed curve represents the radar averaged C_N^2 corrected for moisture and passed through the scintillometer weighting functions of Figure 19

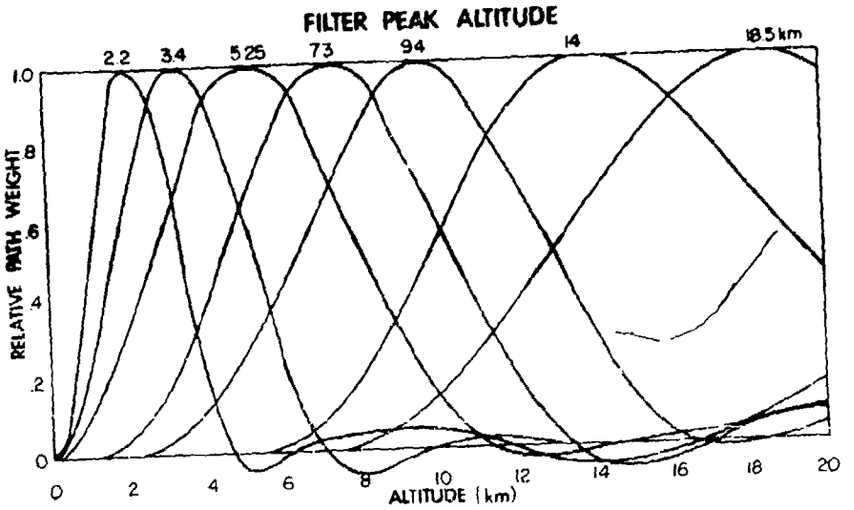

Figure 20. Scintillometer Weighting Functions. The optical scintillometer obtains data over these large weighting functions

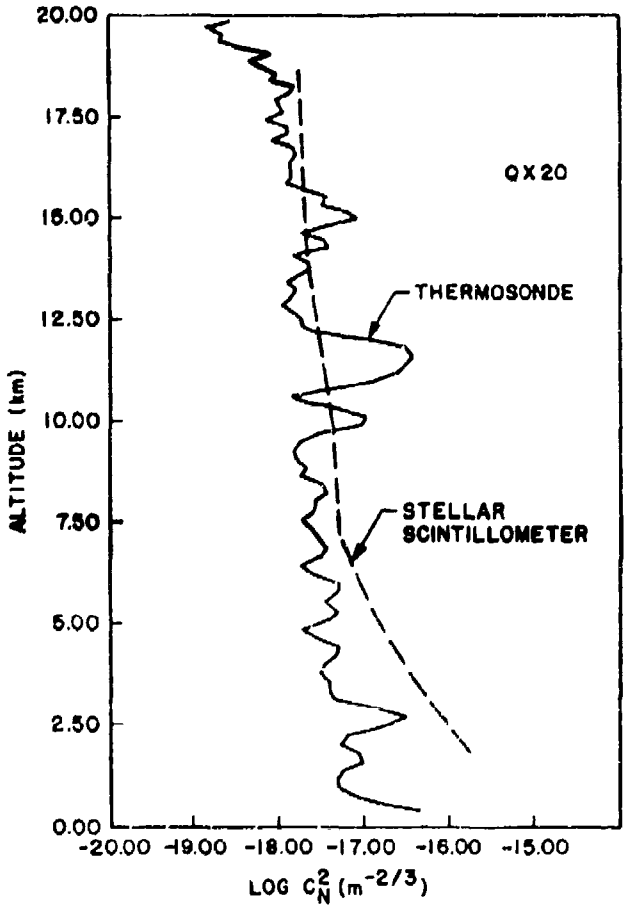

Figure 21. Comparison of Thermosonde C_N^2 and Scintillometer C_N^2 and Scintillometer C_N^2 Profiles. The Thermosonde "raw" C_N^2 data was passed through the scintillometer weighting functions of Figure 19. Although the scintillometer viewed the sky vertically while the thermosonde followed a slant path, the agreement is good

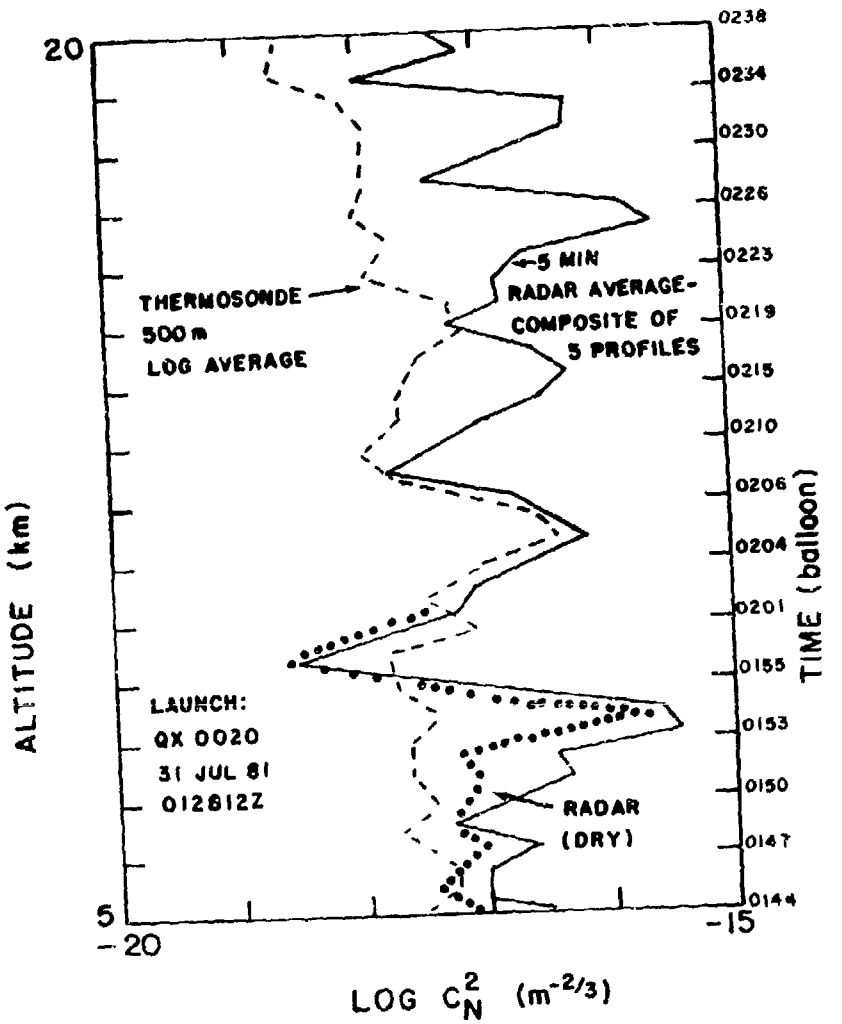

Figure 22. Comparison of Thermosonde C_N^2 and Radar C_N^2 Profiles. The Thermosonde data is averaged over 0.50 km. The Radar data is a time and space composite which attempts to synchronize the time/space coordinates of the Radar and Thermosonde.

References

1. Tatarski, V.I. (1961) Wave Propagation in a Turbulent Medium, McGraw-Hill Co., New York.
2. Titterton, P.J., Mallery, L.E., and Arken, T.A. (1971) Lightweight Thermosonde System, GTE Sylvania, Inc., Final Report, NAS5-11493.
3. GTE Sylvania, Inc. (1972) Lightweight Thermosonde System Model 140 (Instruction Manual), Mountain View, California, B440.
4. Bufton, J.L. (1973) Correlation of microthermal turbulence data with meteorological soundings in the troposphere, J. Atmos. Sci. 30:83-87.
5. Bufton, J.L. (1975) A Radiosonde Thermal Sensor Technique For Measurement of Atmospheric Turbulence, NASA TN D-7867.
6. Curatola, C. (1975) Modifications to GTE Sylvania Thermosonde For Improved Operation, Final Report, AFWL-TR-75-180, ADA 018227.
7. Murphy, G.P. (1981) New Techniques and Devices For Measuring Stratospheric Turbulence, AFGL-TR-81-0128, ADA 102680.
8. Smithells, C.J. (1952) Tungsten, A Treatise on Its Metallurgy, Properties And Applications, Chapman & Hall, London, 3rd ed.
9. Marton, L. (1981) Fluid Dynamics, Academic Press, New York, Vol. 18, Part A, p. 271.
10. Dushman, S. (1962) Scientific Foundations of Vacuum Techniques, John Wiley, New York, p. 47, 2nd ed.
11. Jakob, M. (1949) Heat Transfer, John Wiley, New York, Vol. 1, p. 291.
12. Watkins, B.J. (1981) Millstone Hill Doppler Radar Observations of Winds and Turbulence, Middle Atmospheric Program, Handbook for MAP, Extended abstracts from Int. Sym. on Middle Atm. Dyn. 2:30-36.
13. Ochs, G.R., Lawrence, R.S., and Wang, T. (1976) Stellar scintillation measurement of the vertical profile of refractive – index turbulence in the atmosphere, Proc. Soc. of Photo-optical Inst. Eng. 75:48-54.

14. Endlich, R.M., and Singleton, R.C. (1969) Spectral analysis of detailed vertical wind speeds profiles, J. Atmos. Sci. 26:1030-1041.

15. VanZandt, T.E., Gage, K.S., and Warnock, J.M. (1981) An Improved Model for the Calculation of Profiles of C_N^2 and ε in the Free Atmosphere from Background Profiles of Wind, Temperature, and Humidity, 20th Conf. on Radar Meteorology, (30 Nov. - 3 Dec. 1981).